Title: Smooth muscle expression of RNA editing enzyme *ADAR1* controls activation of RNA sensor MDA5 in atherosclerosis

Authors: Chad S. Weldy[1,2,3,*], Qin Li[4], João P. Monteiro[1], Tim S. Peters[5], Hongchao Guo[6], Drew Galls[7], Wenduo Gu[1], Paul P. Cheng[1,3], Markus Ramste[1], Daniel Li[1], Brian T. Palmisano[1], Disha Sharma[1], Matthew D. Worssam[1], Quanyi Zhao[1], Amruta Bhate[7], Ramendra K. Kundu[1], Trieu Nguyen[1], Michal Mokry[5], Clint L. Miller[8], Sander W. van der Laan[5,8], Jin Billy Li[3,7,†], Thomas Quertermous[1,3,†,*]

Affiliations:
[1]Department of Medicine, Division of Cardiovascular Medicine, Stanford University
[2]Stanford Center for Inherited Cardiovascular Disease, Stanford University
[3]Stanford Cardiovascular Institute
[4]Department of Genetics, University of Pennsylvania
[5]Central Diagnostic Laboratory, University Medical Center Utrecht, University Utrecht, The Netherlands
[6]Cardiovascular Research and Training Institute, University of Utah
[7]Department of Genetics, Stanford University
[8]Department of Genome Sciences, University of Virginia
[†]Co-senior authorship

***Corresponding Authors**:
Chad S. Weldy, MD, PhD
Instructor of Medicine
300 Pasteur Drive, Falk CVRC
Stanford, CA 94305
360-305-8151
weldyc@stanford.edu

Thomas Quertermous, MD
William G. Irwin Professor of Medicine
300 Pasteur Drive, Falk CVRC
Stanford, CA 94305
650-498-5794
tomq1@stanford.edu

Short title: ADAR1 as a causal mechanism of atherosclerosis

One Sentence Summary: Smooth muscle expression of RNA editing enzyme ADAR1 regulates activation of double strand RNA sensor MDA5 in novel mechanism of atherosclerosis.

Abstract:

Mapping the genomic architecture of complex disease has been predicated on the understanding that genetic variants influence disease risk through modifying gene expression. However, recent discoveries have revealed that a significant burden of disease heritability in common autoinflammatory disorders and coronary artery disease (CAD) is mediated through genetic variation modifying post-transcriptional modification of RNA through adenosine-to-inosine (A-to-I) RNA editing. This common RNA modification is catalyzed by ADAR enzymes, where ADAR1 edits specific immunogenic double stranded RNA (dsRNA) to prevent activation of the double strand RNA (dsRNA) sensor MDA5 (*IFIH1*) and stimulation of an interferon stimulated gene (ISG) response. Multiple lines of human genetic data indicate impaired RNA editing and increased dsRNA sensing by MDA5 to be an important mechanism of CAD risk. Here, we provide a crucial link between observations in human genetics and mechanistic cell biology leading to progression of CAD. Through analysis of human atherosclerotic plaque and culture of human coronary artery vascular smooth muscle cells (SMCs) we implicate the SMC to have a distinct requirement for RNA editing, and that MDA5 activation regulates SMC phenotypic modulation. Through generation of a conditional SMC specific *Adar1* deletion mouse model on a pro-atherosclerosis background with additional constitutive deletion of MDA5 (*Ifih1*), and with incorporation of single cell RNA sequencing cellular profiling, we further show that Adar1 controls SMC phenotypic state by regulating Mda5 activation, is required to maintain vascular integrity, and controls progression of atherosclerosis and vascular calcification. Finally, we further corroborate our findings in a large human carotid endarterectomy dataset (Athero-Express) where we show that ISG activation is strongly associated with decreased plaque stability, increased SMC phenotypic modulation, and increased plaque calcification. Through this work, we describe a fundamental mechanism of CAD, where cell type and context specific RNA editing and sensing of dsRNA mediates disease progression, bridging our understanding of human genetics and disease causality.

Main Text:

INTRODUCTION

As coronary artery disease (CAD) is the worldwide leading cause of death[1], there is enormous interest to map the genomic mechanisms of disease, establish biological causality, and accelerate therapeutic drug development. Despite the discovery of hundreds of genomic loci associated with CAD[2-5] the promise of genome wide association studies (GWAS) to identify new mechanisms for treatment outside of lipid lowering therapy has not been fulfilled. Quantitative trait loci (QTL) studies mapping gene expression QTLs (eQTLs) have helped bridge GWAS variants to their molecular mechanisms[6,7]. However, post-transcriptional processes, such as RNA editing, have critical functions in health and disease and genetic determinants of RNA modification are important and poorly appreciated disease mechanisms[8-10]. Catalyzed by adenosine deaminase acting on RNA enzymes (ADARs), adenosine-to-inosine (A-to-I) RNA editing is a highly frequent RNA modification that is evolutionarily conserved across all metazoan species[8,11]. We have recently reported that common genetic variants that modify the frequency of A-to-I RNA editing, loci termed 'editing-QTLs' (edQTL), significantly increase CAD risk as well as numerous other autoinflammatory disorders[12]. This discovery raises the important possibility that genetically determined RNA editing function is a causal mechanism of CAD, yet the biological underpinning of this relationship is unclear.

Foundational work has revealed that ADAR1 (gene symbol *ADAR*) mediated RNA editing is a novel mechanism of inflammation and disease[13-16]. A principal function of ADAR1 is to bind double-stranded RNA (dsRNA) in non-coding repetitive elements and convert adenosines to inosines to facilitate the clearance of dsRNA molecules[17]. This contrasts with ADAR2 (gene symbol *ADARB1*) that serves to edit coding region of transcripts to modify transcript function[11,18]. ADAR1 is ubiquitously expressed across human tissues and its function to edit dsRNA suppresses the sensing of "non-self" dsRNA that is mediated by the cytosolic sensor of dsRNA, MDA5 (gene symbol *IFIH1*) (Fig 1A)[14,19,20]. Mice deficient in Adar1 editing are embryonic lethal due to activation of an interferon-stimulated gene (ISG) response, which is rescued to full life span when Mda5 (*Ifih1*) is also knocked out[14]. In humans, rare variants resulting in loss of function

100 in ADAR1 or gain of function in MDA5 result in two severe and clinically overlapping
101 Mendelian interferon mediated disorders, Acardi Goutières Syndrome and Singleton
102 Merton Syndrome, both of which are characterized by a profound early onset vascular
103 calcification phenotype demonstrating a link between RNA editing and dsRNA sensing
104 in vascular disease[21,22].

105 Common genetic variants that decrease RNA editing and increase CAD risk have
106 similar effects on risk for autoinflammatory disorders such as inflammatory bowel
107 disease and lupus[12]. To further link RNA editing to ISG response in human coronary
108 arteries, risk allele-specific RNA editing was found to be lower and closely predicted an
109 increased interferon gene response (implicating MDA5 activation) in the coronary
110 arteries of patients with CAD[12]. Although prior work has identified ADAR1 as mediating
111 atherosclerotic disease risk through RNA editing of specific RNA transcripts such as
112 *NEAT1* and *CTSS*[23,24], human genetic data corroborates a separate 'axis' of global
113 ADAR1 RNA editing of immunogenic dsRNA to regulate MDA5 activation (ADAR1-
114 dsRNA-MDA5 axis) as a mechanism of atherogenesis (Fig 1A). The relationship of this
115 axis to CAD is further supported by the notable discovery that loss of function variants in
116 *IFIH1* (MDA5) are protective against CAD[25] and that the *IFIH1* locus meets genome
117 wide level significant for association to CAD in GWAS[5].

118 Here, by analyzing human atherosclerotic plaque single cell RNA sequencing
119 (scRNAseq) data, we identified that vascular smooth muscle cells in atherosclerosis
120 express RNA that require ADAR1 mediated RNA editing to evade MDA5 activation at a
121 higher level than other cell types. Through *in vitro* culture of primary human coronary
122 artery smooth muscle cells (HCASMCs) in relevant models, generation of genetic
123 mouse models with conditional deletion of *Adar1* in vascular smooth muscle cells
124 (SMCs) in homozygous loss of function and haploinsufficiency in atherosclerosis,
125 extensive single cell RNA sequencing and histological characterization, with concurrent
126 deletion of *Ifih1* (Mda5), in addition to a large human dataset to evaluate ISG activation
127 and plaque phenotype (Athero-Express), we provide data to support the causality
128 behind the genetic determinants of impaired RNA editing and CAD through MDA5
129 activation. We identify RNA editing in SMC as a mediator of atherosclerosis and by

130 doing so create a new paradigm linking human genetics, epigenomics, and vascular
131 biology to CAD.
132
133 **RESULTS**
134 ***Expression of immunogenic RNA within vascular SMCs in human atherosclerotic***
135 ***plaque***
136 Activation of MDA5 is dependent on the concentration of specific RNA molecules that
137 are prone to the formation dsRNA structures and form a pattern recognized by MDA5[26].
138 By combining our data from experimental *in vitro* models[27] along with human genetic
139 edQTL analysis[12], we generated a putative list of 629 high probability human RNA
140 molecules that are 'immunogenic' and require RNA editing to evade sensing by MDA5
141 (Table S1). Given the relationship between edQTLs and CAD, we evaluated human
142 scRNAseq data from carotid atherosclerotic plaque[28] to determine if there is a cell type
143 specific expression of these immunogenic RNA. We determined cell clusters and cell
144 types (Fig 1B) and generated a cell module 'score' that summates the expression of all
145 629 high probability 'immunogenic' RNA. Human SMCs expressed these immunogenic
146 RNA at a higher level compared to all other cell types (Fig 1C). This observation may
147 suggest a distinct role for SMCs in mediating RNA editing within the vessel wall.
148
149 ***SMC phenotypic modulation and ISG induction in atherosclerosis***
150 The formation of atherosclerotic plaque and vascular calcification involves SMCs
151 undergoing a process of epigenetic reprogramming, termed "phenotypic
152 modulation"[29,30]. In this process, SMCs dedifferentiate, down-regulate lineage marker
153 expression, and migrate into the atheroma where these cells then proliferate and
154 differentiate into different progenies that affect the biology of the plaque. Using SMC
155 lineage tracing mouse models of atherosclerosis with single cell RNA and ATAC
156 sequencing of the aortic root, we have previously shown that numerous CAD risk genes
157 mediate disease risk through modification of this phenotypic modulation, including
158 *TCF21*, *ZEB2*, *AHR*, *PDGFD* and *SMAD3*[31-35]. Mature SMCs will undergo phenotypic
159 modulation to a more 'fibroblast like' fibromyocyte (FMC) and then into a calcification
160 promoting chondromyocyte (CMC)[33] phenotype in the setting of disease.

161 Given SMCs express immunogenic RNA at a higher level than other cell types,
162 we hypothesized that insufficient RNA editing and dsRNA sensing could be identified as
163 expression of key ISGs in the SMC population. We performed a subset analysis of the
164 SMC population in this dataset[28] where clustering revealed 4 major clusters (cluster '0',
165 '1', '2', and '3')(Fig 1D). SMCs undergo a process of downregulation of the mature SMC
166 marker *MYH11* (Fig 1E, cluster 2 vs 0 — -2.92 log2 fold change, adjusted *p* value
167 1.98E-290) with upregulation of FMC/CMC markers including *TNFRSF11B*, *HAPLN1*
168 and *LUM* (ex. *TNFRSF11B* Fig 1F, cluster 2 vs 0 — 1.52 log2 fold change, adjusted *p*
169 value 3.07E-26) as SMCs transition from mature SMC cluster '2' to FMC/CMC cluster
170 '0' — a finding we have previously reported[33]. However, findmarker analysis of these
171 clusters identified numerous ISGs as top markers of the FMC/CMC cluster '0', including
172 *ISG15*, *IFI35*, *IFI16*, *IFI27*, *IFIT3* (ex. *ISG15*, *IFI35*, *IFI16;* adj *p* value 3.94E-21, 2.60E-
173 27, 2.63E-64, respectively; Fig 1G-J) (FindMarker results in Table S2). This finding may
174 suggest dsRNA sensing by MDA5 with phenotypic modulation.
175 To investigate if ISG induction with SMC phenotypic modulation is conserved in
176 mouse models of atherosclerosis, we evaluated our previously published
177 comprehensive integrated dataset of multiple single cell transcriptomic experiments[36]. In
178 this dataset, we determined the transcriptomic profiles in the aortic root of lineage
179 traced SMCs in hyperlipidemic models of atherosclerosis[36]. We observed that in
180 comparing between 0 and 16 weeks of high fat diet, SMCs underwent significant
181 phenotypic modulation, marked by downregulation of SMC contractile marker *Myh11*
182 (Fig 1K; -0.73 log2 fold change, $p < 2E-16$), with upregulation of *Col2a1* (Fig 1L; 3.29
183 log2 fold change, $p < 2E-16$), a marker of chondromyocyte formation. With this
184 phenotypic transition, we observed significant upregulation of ISGs including *Isg15* (Fig
185 1M; 0.29 log2 fold change, $p < 2E-16$) and *Ifit3* (Fig 1N) in these phenotypically modified
186 SMCs. These cells lie at the juncture between FMC and CMC formation and expression
187 was absent in mature SMCs prior to phenotypic modulation.
188
189 ***SMC ADAR1 and MDA5 expression in atherosclerosis in mice***
190 To understand the expression patterns of *ADAR* and *IFIH1* (MDA5) in atherosclerosis
191 SMC phenotypic modulation, we evaluated the expression of *ADAR* and *IFIH1* in this

192 human carotid atherosclerosis dataset where we observed no differences in the
193 expression of either *ADAR* or *IFIH1* across the different SMC subsets (Fig S1A-B)($p >$
194 0.05). We then evaluated if expression of *ADAR* and *IFIH1* varied significantly across
195 cell types in this human carotid atherosclerosis dataset, where we observed that
196 expression of *ADAR* appeared largely consistent between SMCs, Endos, Fibros, and
197 other immune cells, however *IFIH1* expression appeared highest in endothelial cells,
198 followed by macrophage and SMCs (Fig S1C).
199 With evaluation of our comprehensive SMC lineage traced mouse dataset
200 comparing week 0 and week 16, we observed a small increase in *Adar* and *Ifih1* at 16
201 weeks compared to the 0-week baseline (Fig S1D-F, *Adar* 1.26 fold p=2.2e-7; *Ifih1* 2.01
202 fold $p<2e-16$). At the 16-week timepoint, *Adar* expression appears largely consistent
203 across SMC populations with phenotypic modulation, however *Ifih1* (Mda5) increases
204 significantly at the FMC/CMC junction as observed with other ISGs (Fig S1D-F).
205
206 ***ADAR1 controls global RNA editing and ISG response in human coronary artery***
207 ***smooth muscle cells***
208 To investigate ADAR1 in human SMCs, we used an *in vitro* model of phenotypic
209 modulation with primary human coronary artery smooth muscle cells (HCASMCs) and
210 knocked down (KD) *ADAR* (ADAR1) and *IFIH1* (MDA5) with siRNA transfection paired
211 with bulk RNA sequencing (RNAseq). In this model (Fig S2A), we cultured HCASMCs to
212 confluency, treated with siRNA for 48 hours, and then transitioned to serum free
213 medium (serum starvation) to induce a mature SMC phenotype marked by high
214 expression of SMC markers (*e.g. ACTA2*, *CNN1*). Following 48 hours of serum
215 starvation, cells were stimulated with either serum replete medium or maintained in a
216 serum free medium for 48 hours. With serum stimulation, HCASMCs subsequently
217 downregulated expression of mature SMC markers, a phenotype akin to phenotypic
218 modulation in the SMC to FMC transition in atherosclerosis[33].
219 With RNAseq data we inferred total RNA editing by detection of G base
220 sequences at RNA editing sites as we have done previously (Fig S2B)[12,37]. We
221 observed a notably strong linear relationship between *ADAR* expression and global

222 RNA editing frequency (r^2=0.9509, *p<0.0001*) (Fig S2B&C). Intriguingly, RNA editing
223 frequency significantly decreased with serum stimulation alone (Fig S2C).
224 *ADAR* siRNA transfection in serum starved conditions induced a significant gene
225 expression response with 6,351 differentially expressed genes (*FDR <0.05*) (Fig S2D).
226 Top upregulated genes were interferon stimulated genes (ISGs) including *ISG15, IFI6*,
227 *IFI44L*, *IFIT2*, and *IFIT1* (Fig S2D). With transfection of both *ADAR* (ADAR1) and *IFIH1*
228 (MDA5) siRNAs we observed that co-KD of *IFIH1* blocked the majority of the gene
229 expression response (Fig S2E).
230 With serum stimulation (representing phenotypic modulation) we observed *ADAR*
231 KD induced a much greater effect than seen with serum starvation with 12,747
232 differentially expressed genes (*FDR <0.05*) (Fig 2F). This effect was characterized with
233 a dominant ISG response and appeared nearly entirely dependent on activation of
234 MDA5 (Fig 2G). When using principal component analysis (PCA) of bulk RNAseq data
235 for each treatment group, we observed that the two dominant principal components
236 tracked with MDA5 activation (PC1) and serum stimulation (PC2), where serum starved
237 cells with *ADAR* KD produced an outwards shift on PC1, and then returned to near
238 baseline with co-KD of *IFIH1* (Fig 2H). With serum stimulation, there was an upwards
239 shift on PC2, and an even greater shift on PC1 with *ADAR* KD, and a return to baseline
240 with co-KD of *IFIH1* (Fig 2H). These findings highlight that the dominant effect of
241 impaired RNA editing in HCASMCs is driven by activation of MDA5 and SMC cell state.
242
243 ***ADAR1 and MDA5 regulate SMC maturation and key CAD transcription factors in***
244 ***phenotypic transition***
245 In this HCASMC model of phenotypic transition, we observed that serum stimulation
246 downregulated mature SMC markers including *ACTA2* and *CNN1* (Fig S2I&J).
247 However, we also observed that *ADAR* KD alone downregulated these SMC markers,
248 an effect that was accentuated with serum stimulation (Fig S2I&J). Using *ISG15*
249 expression as a marker of ISG activation, *ADAR* KD induced an increase in *ISG15*
250 expression (Fig S2K), an effect that was enhanced with serum stimulation and entirely
251 blocked with co-KD of *IFIH1* (MDA5) (Fig S2K). Interestingly, numerous other key

252 transcription factors with known functions in SMC maturation and risk of CAD (*i.e. KLF4*,
253 *EGR1*, and *ATF3*)[38] were similarly affected with *ADAR* KD (Fig S2L-2M).
254 Notably, classical interferon genes interferon α, β, and γ (i.e. *IFNA1*, *IFNB1,*
255 *IFNG*) were either not expressed (*IFNA1* & *IFNG*), or minimally affected by *ADAR* KD in
256 an MDA5 dependent mechanism (*IFNB1*) (Fig S3A-C) with similar minimal effect on the
257 key IFN receptor, *IFNAR1* (Fig S3D). Top KEGG pathways of upregulated genes
258 indicated a global viral sensing and inflammatory response, including "TNF signaling
259 pathway", "Influenza A", "NOD-like receptor pathway", and "EBV infection", as well as
260 "Lipid and atherosclerosis" (Fig S3E). GO biological processes similarly revealed
261 "Defense Response to Virus" as the top process (Fig S3F). Downregulated pathways
262 highlighted "Ribosome", "Focal Adhesion", and "ECM-receptor interaction" (Fig S3G)
263 and GO terms suggested downregulation of RNA and protein processing with
264 "Cytoplasmic translation" and related terms (Fig S3H).
265
266 ***Global RNA editing is decreased in HCASMC following phenotypic modulation in***
267 ***vitro***
268 In the evaluation of global RNA editing frequency in HCASMC with phenotypic
269 modulation (serum stimulation) with control, *ADAR,* or *ADAR* + *IFIH1* KD, we observed
270 that serum stimulation alone appeared to decrease total RNA editing (Fig S2C). Given
271 we see serum stimulation to increase MDA5 activation with *ADAR* KD, this suggests a
272 potential interaction between phenotypic modulation, decreased RNA editing, and
273 dsRNA formation. To better understand this relationship, we performed a genome wide
274 RNA editing site specific comparison in serum starved and serum stimulated HCASMC
275 (Fig S4). In comparing the mean RNA editing level for each RNA editing site in control
276 siRNA treated cells in serum starved and serum stimulated conditions, we observed a
277 significant shift where serum stimulated cells have an overall decrease in RNA editing
278 (Fig S4A). Although no specific RNA editing site met genome wide level significance,
279 there was a significant overall net effect to decrease RNA editing frequency across
280 hundreds of RNA editing sites. To evaluate the effect of *ADAR* KD we performed this
281 editing site specific analysis in the *ADAR* KD with concurrent *IFIH1* KD (minimize the
282 effect of MDA5 activation on ADAR1 editing) that revealed a massive reduction in RNA

editing with *ADAR* KD in both serum starved, and serum stimulated conditions (Fig S4B&C). From this analysis, we then identified 1,101 differentially edited sites (DES) across 219 genes (Fig S4D&E) that are ADAR1 dependent. Most of these DES are shared between serum starved and serum stimulated conditions (Fig S4D&E), however we identified 226 sites within 38 genes that are distinct to serum stimulated conditions, and 357 sites within 49 genes that are distinct to serum starved conditions. Evaluation of these genes show no consistent biological pattern where gene ontology enrichment analysis shows no significant pathways (data not shown), however several genes (*TCTA, SWAP70, FN1, GGCX*) have been identified to reside at loci that meet genome wide level significance for CAD[5]. These data implicate specific genes that may be responsible for this enhanced MDA5 activation seen with serum stimulation.

To understand how serum stimulation may influence the overall expression of immunogenic RNA, we analyzed the expression change of the 629 previously identified immunogenic RNA (Table S1) and performed differential gene expression analysis. We observed that in HCASMC, serum stimulation elicited a notable change in gene expression of these selected genes with 82% differentially expressed (Fig S4G), however there appeared to be a relative balance between upregulated (249) and downregulated (239) genes. We hypothesized that the overall expression of these combined immunogenic RNA may have significance, where we measured the overall expression of all 629 immunogenic RNA by normalized RNAseq read counts. We observed that serum stimulation did not change the overall expression of the total immunogenic RNAs by combined RNA read count, however we did observe that with *ADAR* KD and MDA5 (*IFIH1*) activation, the expression of these RNAs trended down in the serum starved cells (p=0.11), and then significantly decreased in the serum stimulated cells (p=0.0022) in an MDA5 dependent mechanism (Fig S4H). We then looked at two distinct immunogenic RNA that colocalize with CAD GWAS where serum stimulation results in upregulation, *SWAP70* and *TCTA*. We observe that serum stimulation leads to upregulation, however *ADAR* KD blocks this effect in an MDA5 (*IFIH1*) dependent mechanism (Fig S4I&J). These data may suggest that MDA5 activation can regulate the global expression of immunogenic RNA.

314 ***TGFβ attenuates MDA5 and ISG activation in HCASMC***

315 As we observed *ADAR* and *IFIH1* (MDA5) to have distinct effects on HCASMC
316 response to serum stimulation (a "synthetic" response), we aimed to further understand
317 how *ADAR*, *IFIH1*, and *PKR* — a key ISG that acts to control cellular signaling following
318 MDA5 activation[39] — may further regulate HCASMC response to TGFβ as a
319 'contractile' response. We cultured HCASMC to confluency, treated with siRNA for 48
320 hours, and transitioned cells to a serum free condition for 72 hours. We then stimulated
321 cells with TGFβ (10ng/mL) or control for 72 hours before we isolated RNA and
322 performed quantitative PCR. When evaluating expression of key ISGs such as *ISG15*,
323 we observed that TGFβ treatment significantly blunted the effect of *ADAR* KD, where a
324 25-fold upregulation of *ISG15* with *ADAR* KD in serum starved conditions was limited to
325 less than 10-fold upregulation with TGFβ treatment (Fig S5A). Upregulation of *ISG15*
326 was entirely blocked with KD of *IFIH1* (MDA5) and markedly reduced with *PKR* KD (Fig
327 S5A). This finding suggests activation of *PKR* itself further activates the ISG response.
328 In our prior serum stimulation study, *ADAR* KD induced a marked upregulation of *IFIH1*
329 (MDA5) that was exacerbated with serum stimulation in a pattern that was consistent
330 with all other ISGs (Fig S5B). However, TGFβ treatment reduced this effect of *ADAR*
331 KD (Fig S5C). In control cells, we observed that concurrent *PKR* KD further blunted the
332 activation of *IFIH1* (MDA5)(Fig S5C). We then evaluated expression of *PKR* where we
333 found *PKR* to similarly be upregulated by *ADAR* KD, however this effect was
334 significantly reduced with TGFβ treatment (Fig S5D) and in control cells was entirely
335 blocked with *IFIH1* (MDA5) KD (Fig S5D).

336 To understand if the effect of TGFβ to blunt the ISG response is dependent on
337 canonical TGFβ TFs such as SMAD3, we performed additional experiments with
338 concurrent *SMAD3* KD and evaluated the expression if *ISG15* and *IFIH1*. Interestingly,
339 we observed that *SMAD3* KD itself attenuated the upregulation of both *ISG15* and *IFIH1*
340 (Fig S5E&F) with concurrent *ADAR* KD, suggesting that SMAD3 is playing a role to
341 activate ISG response with *ADAR* KD. However, the effect of TGFβ treatment appeared
342 to be the same despite *SMAD3* KD (Fig S5E&F). This may suggest that SMAD3 and
343 TGFβ have distinct yet contrasting roles in regulating ISG induction, implicating
344 alternative, non-canonical TGFβ signaling pathways to mediate this effect.

345 In comparing the effect of serum stimulation or TGFβ treatment on *ADAR*
346 expression, we observed that serum stimulation induced a small increase in *ADAR*
347 expression (~1.2 fold, Fig S5G)(similar to what we observed *in vivo* during
348 atherosclerosis, Fig S1), whereas TGFβ treatment produced a somewhat greater 2-fold
349 upregulation of *ADAR* (Fig S5H). At this timepoint, 8 days after siRNA treatment, *ADAR*
350 expression in the *ADAR* KD treatment was found to have normalized in a manner
351 dependent on *IFIH1* (MDA5), however not dependent on PKR, indicating that MDA5
352 activation is stimulating a compensatory upregulation of *ADAR* (Fig S5H).
353 To then understand how MDA5 and PKR may be regulating HCASMC response
354 to TGFβ and phenotypic modulation, we evaluated the expression of the mature SMC
355 contractile marker *ACTA2* as well as TGFβ responsive gene *PI16*. We observed that
356 TGFβ stimulation downregulates *ACTA2* in a manner similar to *ADAR* KD. In addition,
357 downregulation of *ACTA2* with *ADAR* KD in control cells was dependent on MDA5
358 (*IFIH1*) and to a lesser extent *PKR* (Fig S5G). However, the effect of TGFβ to
359 downregulate *ACTA2* was entirely independent of *ADAR*, *IFIH1*, or *PKR* (Fig S5G). We
360 found that TGFβ treatment significantly upregulated *PI16*, however this effect was
361 significantly blunted with KD of *ADAR*, in a manner dependent on both *IFIH1* (MDA5)
362 and *PKR* (Fig S5H), suggesting activation of MDA5 and subsequently PKR may
363 regulate SMC response to TGFβ.
364
365 ***ADAR1 and MDA5 regulate the transcriptomic and inflammatory response to***
366 ***calcification in vitro***
367 To model SMC calcification *in vitro*, we cultured an immortalized HCASMC line under
368 high calcium/phosphate culture conditions as has been previously reported[40]. In this
369 model, SMCs begin to form deposits that stain with Alizarin red, consistent with calcium
370 crystals and has been proposed to represent vascular calcification[40]. Following siRNA
371 transfection for 48 hours, we cultured cells for 7 days with pro-calcification medium
372 under low serum (1%) conditions and performed bulk RNAseq. After 7 days,
373 calcification deposits became visible, however with *ADAR* KD, there was a significant
374 phenotypic change with increased cell death and increased density of calcium deposits
375 — an effect that was blocked with co-KD of *IFIH1* (Fig S6A&B). Calcification medium

376 under scramble siRNA treatment promoted a significant gene expression response with
377 584 differentially expressed genes (*FDR <0.05*) (Fig S6C). Top upregulated genes
378 include numerous BMP related signaling genes including *FBLN5*, *FMOD*, and
379 *RANBP3L* (Fig S6D-F), effects that have been previously reported[40]. However, with
380 *ADAR* KD this effect was blunted in an MDA5 dependent mechanism (Fig S6D-F).
381 Calcification did not overtly activate MDA5 as measured by expression of ISGs
382 (i.e. *ISG15*)(Fig S6G&H), however, *ADAR* KD modified the HCASMC inflammatory
383 response to calcification. Calcification had minimal effect on expression of NFκB
384 (*NFKB1*), however with *ADAR* KD *NFKB1* is modestly upregulated and is further
385 upregulated with calcification in *ADAR* KD cells, an effect blocked with co-KD of *IFIH1*
386 (Fig S6I). This observation revealed a unique relationship where calcification induced a
387 distinct proinflammatory effect only with concurrent *ADAR* KD and MDA5 activation.
388 Similar effects were observed for numerous proinflammatory signaling and matrix
389 proteins including *JUND*, *MMP1*, and *MMP10* (Fig S6J-L).
390
391 ***SMC specific Adar1 maintains vascular integrity and survival in vivo***
392 Although prior reports have implicated SMC specific RNA editing in mediating
393 phenotypic response[41,42], the relationship between deficient SMC RNA editing, MDA5
394 activation, vascular inflammation, and atherosclerosis has not been investigated. To
395 understand how homozygous deletion of *Adar1* within SMCs influence vascular
396 homeostasis, we bred a mouse model with four distinct alleles, including *Adar1*$^{fl/fl}$ (exon
397 7-9), a tamoxifen inducible SMC specific Cre-recombinase (*Myh11*^{CreERT2}), a lineage
398 tracing fluorophore (*ROSA*^{tdTomato}), on a hyperlipidemic pro-atherosclerosis genetic
399 background (*ApoE*$^{-/-}$) (Fig 2A). A total of 56 mice were treated, comparing *SMC-Adar1*$^{-/-}$,
400 *SMC-Adar1*$^{-/+}$ (*Adar1*$^{fl/WT}$, *Myh11*^{CreERT2}, *ROSA*^{tdTomato}, *ApoE*$^{-/-}$), and control (*Adar1*$^{WT/WT}$,
401 *Myh11*^{CreERT2}, *ROSA*^{tdTomato}, *ApoE*$^{-/-}$) genotypes. We observed that at day 4, *SMC-*
402 *Adar1*$^{-/-}$ mice became notably ill as characterized by weight loss, piloerection, and a
403 hunched posture, a phenotype that was not present in *SMC-Adar1*$^{-/+}$ or control genotype
404 animals. We observed mortality in the *SMC-Adar1*$^{-/-}$ mice at this time and by 14 days,
405 10/20 (50%) mice had died (Fig 2B). A recent report while this manuscript was in review
406 has further supported this role of SMC specific *Adar1* to maintain survival and vascular

407 integrity[43]. Gross dissection and visual inspection of *SMC-Adar1*$^{-/-}$ mice did not reveal
408 prominent findings of the lungs, heart, or intestines however visual appearance of the
409 aorta suggested petechial hemorrhage and erythema (Fig 2C). H&E staining (Fig
410 2D&E), fluorescent imaging (Fig 2F&G), bright field imaging (Fig 2H), Cd68
411 immunostaining (Fig 2I), and Masson's trichrome staining (Fig 2J) of ascending and
412 descending aortic tissue in 6 *SMC-Adar1*$^{-/-}$ mice revealed a loss of elastin organization
413 (present in 6/6 mice), dissociation of the matrix at the adventitial aspect with associated
414 'ballooning' out and separation of layers (present in 3/6 mice), with evidence of
415 intramural hemorrhage (present in 2/6 mice) (Fig 2D-H, Fig S7). These sites of
416 ballooning occurred with complete loss of tdTomato SMCs at the adventitial aspect (Fig
417 2F&G). H&E staining of the aorta confirmed severe loss of organization of the elastin
418 matrix and evidence of intravascular hemorrhage with further discovery of dense cellular
419 infiltrate into the adventitia (Fig 2D&E). These patterns were not observed in control
420 mice (Fig 2E). Immunostaining for CD68 revealed macrophage cell infiltration from the
421 luminal as well as the adventitial aspect of the vessel wall (Fig 2I). Additional Masson's
422 trichrome stain to evaluate for fibrosis revealed evidence of intra-medial collagen
423 deposition (Fig 2J).
424 In this model, there was a rapid and early inflammatory response that resulted in
425 profound weight loss and mortality. Although the cause of death was not immediately
426 apparent, as gross examination and H&E sections of liver, lung, and heart were
427 nonrevealing, the acute systemic inflammatory response is likely eliciting death through
428 a multifactorial mechanism akin to a systemic inflammatory response. There was no
429 evidence of aortic rupture as a cause of death. However, mice that survived this period
430 remained underweight (15-18 grams) and ill in appearance until ~7 months of age.
431 Importantly, no mice that were taken past this 2-week timepoint regained weight or lived
432 a normal lifespan. Dissection of mice at this 7-month timepoint demonstrated dense
433 fecal impaction of the large intestine, consistent with bowel obstruction, a finding not
434 seen at earlier timepoints.
435
436 ***Haploinsufficiency of MDA5 is sufficient to protect against mortality with SMC***
437 ***Adar1*$^{-/-}$ *mice***

438 Our *in vitro* work indicates MDA5 to be the principal mediator of downstream signaling
439 with *ADAR1* KD in SMC, however it remains unclear if this relationship is true *in vivo*. In
440 addition, it is unclear if only partial inhibition of MDA5 can prevent overt ISG activation,
441 a model more akin to what might be achieved with future pharmacologic inhibition. To
442 test this, we bred the SMC *Adar1* KO mouse onto a constitutive KO of *Ifih1* (Mda5) on
443 both a heterozygous and homozygous background generating mice that are *SMC-*
444 *Adar1*$^{-/-}$ + *Mda5*$^{-/+}$ (*Adar1*$^{fl/fl}$, *Ifih1*$^{-/+}$, *Myh11*^{CreERT2}, *ROSAtdTomato*, *ApoE*$^{-/-}$) and *SMC-*
445 *Adar1*$^{-/-}$ + *Mda5*$^{-/-}$ (*Adar1*$^{fl/fl}$, *Ifih1*$^{-/-}$, *Myh11*^{CreERT2}, *ROSAtdTomato*, *ApoE*$^{-/-}$). Following
446 the same model as shown previously (Fig 2), we performed an additional experiment
447 using litter-mate controlled mice with tamoxifen treatment for a total of 32 mice (12
448 SMC-*Adar1*$^{-/-}$, 8 *SMC-Adar1*$^{-/-}$ + *Mda5*$^{-/+}$, and 12 *SMC-Adar1*$^{-/-}$ + *Mda5*$^{-/-}$). Mice that were
449 homozygous SMC *Adar1* KO with MDA5 WT had severe weight loss and significant
450 mortality, with 10/12 (83%) *SMC-Adar1*$^{-/-}$ mice dying prior to the 14-day timepoint and
451 greater than 30% loss of total body weight by 7 days for the 6 mice that survived to the
452 7-day timepoint (Fig 3A-C). Both *SMC-Adar1*$^{-/-}$ + *Mda5*$^{-/+}$ and *SMC-Adar1*$^{-/-}$ + *Mda5*$^{-/-}$
453 mice showed minimal weight loss, no mortality, and visually appeared largely unaffected
454 by *Adar1* KO at this 2-week timepoint (Fig 3A-D). *SMC-Adar1*$^{-/-}$ + *Mda5*$^{-/+}$ mice have
455 been taken out to 24 weeks following tamoxifen dosing and continue to show minimal
456 phenotype, demonstrating that MDA5 is required to initiate this severe phenotype with
457 SMC *Adar1* KO. Histological evaluation of aortic tissue from *SMC-Adar1*$^{-/-}$, *Mda5*$^{-/+}$ mice
458 show that aortic cross section, aortic media, and elastin structures are indistinguishable
459 from control mice (Fig S8). Intriguingly, a portion of both *SMC-Adar1*$^{-/-}$, *Mda5*$^{-/+}$ and
460 *SMC-Adar1*$^{-/-}$, *Mda5*$^{-/-}$ mice (2/8 and 4/12, respectively) did lose significant weight within
461 the first week, however had significant weight recovery by week 2 (Fig 3C). This
462 suggests that although MDA5 deletion protects against mortality and any major
463 phenotype, that alternative dsRNA receptors such as RIG-I may be mediating a partial
464 inflammatory response.
465
466 ***Single cell RNA sequencing reveals SMC Adar1 controls ISG activation,***
467 ***phenotypic response, and macrophage infiltration into the vessel wall***

468 To further characterize the vascular response of SMC specific *Adar1* KO in mouse, we
469 performed single cell RNA sequencing (scRNAseq) of the aortic root and ascending
470 aorta of *SMC-Adar1*$^{-/-}$ mice at day 14 following tamoxifen dosing. With a total of 10
471 individual scRNAseq captures, we characterized over 50,000 cells with high sequencing
472 depth (>50K reads per cell). Using dimensionality reduction with UMAP as we have
473 done previously[44,45], we observed *SMC-Adar1*$^{-/-}$ aortic cells to have a dramatic
474 transcriptomic change in comparison to control genotype (Fig 4A). Cluster analysis
475 identified 13 main clusters, including 3 SMC clusters — a control SMC cluster marked
476 by mature contractile markers (i.e. *Myh11* and *Cnn1*), and two SMC clusters that
477 represented cells with distinct transcriptomic signatures secondary to SMC *Adar1* KO
478 that are marked by tdTomato (clusters SMC_cAdar1_KD1; SMC_cAdar1_KD2) (Fig
479 4B&C) (Findmarker gene analysis in Table S3). Genes expressed by cells in these two
480 clusters were found to show gene ontology (GO) enrichment for terms related to
481 'response to interferon beta', 'response to virus', 'defense response to virus' as top GO
482 terms (Fig S9). Using *Isg15* as a marker of MDA5 activation, clusters
483 SMC_cAdar1_KD1 and SMC_cAdar1_KD2 were marked by notably high expression of
484 *Isg15* (Fig 4D). To validate this finding and characterize the location of *Isg15*
485 expression, we performed RNAscope on aortic tissue from *SMC-Adar1*$^{-/-}$ mice. We
486 observed robust *Isg15* expression within the vessel wall that was highest at the luminal
487 aspect of the media, with additional expression within the adventitia (Fig 4E).
488 Within tdTomato lineage traced SMCs, conditional *Adar1* KO produced marked
489 gene expression changes with 2,382 differentially expressed genes (*FDR<0.05,*
490 *log2FC>0.1*), with notable increase in ISGs. In comparing clusters SMC_cAdar1_KD1
491 and SMC_cAdar1_KD2, SMC_cAdar1_KD2 was marked by higher expression of
492 numerous inflammatory signaling genes (i.e. *Isg15*, *Ccl5*, *Cxcl10*) (Fig S10A).
493 Importantly, consistent with our *in vitro* findings (Fig S3A-D), there was only
494 modest activation of classical interferon genes with no observed expression of *Ifna1* and
495 minor activation of *Ifnb1* (Fig 4F). Similarly, we observed minimal expression of IL6
496 family cytokines (i.e. *Il6*) with *SMC-Adar1*$^{-/-}$ (Fig S10B). The minimal expression of these
497 markers appeared limited to the more proinflammatory SMC_cAdar1_KD2 cluster. In
498 addition, consistent with our *in vitro* findings, we observed that SMC *Adar1* KO led to

499 downregulation of mature SMC markers (Fig S10C). By comparing the three major SMC
500 clusters, expression of *Cnn1* and *Myh11* decreased in a pattern consistent with
501 increasing MDA5 activation (Fig S10C).
502 There was a new distinct fibroblast population seen only with SMC *Adar1*$^{-/-}$ and is
503 marked by ISGs and high expression of *Ly6a* (Sca1) (Fig 4B, Fig S10D), consistent with
504 a proinflammatory adventitial fibroblast population[46]. Similarly, in SMC *Adar1*$^{-/-}$ there
505 was a loss of cells within the 'Fibro_1' cluster that was only seen in controls (Fig 4B),
506 suggesting a dynamic shift in gene expression from resident fibroblasts to this new
507 reparative and inflammatory cell cluster. In addition, there was a large infiltrating
508 macrophage population marked by high *Cd68* (resident macrophage cluster – 'Mac',
509 infiltrating macrophage cluster – 'Mac_2') (Fig 4B, Fig S10E) with an additional small T
510 cell population with SMC *Adar1*$^{-/-}$ marked by high *Gzma*, *Cd3g*, and *Cd52*, suggestive of
511 a cytotoxic T lymphocyte (CTL) population (Fig 4B, Fig S10F). These data indicate that
512 with loss of *Adar1* within SMCs, a profound vascular response occurs throughout the
513 vessel wall that is coordinated by SMCs.
514
515 ***Receptor-ligand interaction modeling implicates CCL5:CCR5 to coordinate***
516 ***macrophage infiltration in SMC-Adar1$^{-/-}$ mice***
517 To better understand the cell-cell communications that mediate this response, we
518 performed an inference analysis of cell-cell communication focused on receptor-ligand
519 interactions (CellChat)[47]. This analysis revealed that with SMC *Adar1*$^{-/-}$, SMC clusters
520 SMC_cAdar1_KD1 and SMC_cAdar1_KD2 are notably high outward senders of CCL
521 signaling markers (Fig 4G). When interrogating the specific signaling pairs, Ccl5:Ccr5
522 was the dominant interaction (Fig 4H). A circos plot depicting Ccl5:Ccr5 interaction
523 strength revealed dominant outward interaction arising from SMC_cAdar1_KD1 and
524 SMC_cAdar1_KD2 clusters with key receiving clusters being resident macrophage,
525 infiltrating macrophage, and T cell populations (Fig 4I). Feature plots of Ccl5 and Ccr5
526 further revealed the distinct expression of Ccl5 within SMCs following *Adar1* KO and
527 Ccr5 within macrophage populations (Fig 4J&K). Evaluation of the next top 3 interaction
528 pairs (Ccl2:Ccr2; Ccl4:Ccr5, Ccl7:Ccr2) suggested that following Ccl5:Ccr5 interaction,
529 Ccl2 and Ccl7 arising from SMC_cAdar1_KD2, Fibro_Sca1_hi, and macrophage cell

530 populations appeared to interact with Ccr2 within macrophage and T lymphocyte
531 populations (Fig S10G-L). These data suggested that Ccl4 from resident and infiltrating
532 macrophage clusters further signaled through Ccr5 on these same cell clusters (Fig
533 S10J&K). Activation of CCR5 has been previously identified as a key regulator of
534 antiapoptotic signaling in macrophage cells in response to viral infection[48]. Our
535 observation provides a unique insight that following the loss of SMC *Adar1*, Ccl5:Ccr5
536 acts as a dominant regulator of macrophage infiltration and macrophage cell survival.
537
538 ***Homozygous deletion of MDA5 (Ifih1) prevents transcriptomic effect of SMC-***
539 ***Adar1 KO seen with single cell RNA sequencing***
540 Our data indicates that loss of SMC *Adar1* elicits severe vascular effect and mortality
541 due to dsRNA activation of MDA5 (Fig 3). Further, our *in vitro* HCASMC data suggests
542 that loss of *ADAR1* with concurrent MDA5 KD produces only a minor effect on cellular
543 transcriptome (Fig S2). However, it is unclear if this is true *in vivo* and there remains
544 question as to if loss of RNA editing by ADAR1 may mediate significant transcriptomic
545 effect despite concurrent MDA5 deletion. To investigate this, we performed additional
546 scRNAseq captures in 9 *SMC-Adar1*$^{-/-}$*, Mda5*$^{-/-}$ mice at this same timepoint of 14-days
547 post tamoxifen as previously performed, for a total of 6 scRNAseq captures. Data was
548 integrated together with control and *SMC-Adar1*$^{-/-}$ captures (16 total sequencing
549 libraries). Remarkably, UMAP visualization of single cell transcriptomic data from *SMC-*
550 *Adar1*$^{-/-}$*, Mda5*$^{-/-}$ mice show nearly identical pattern compared to control (S11A).
551 Infiltrating macrophage and T cell populations and Sca1-hi fibroblast populations are no
552 longer present. When evaluating expression of key ISGs such as *Isg15* and *Ccl5*,
553 homozygous *Mda5* (*Ifih1*) KO prevents the entirety of ISG induction across all cell types
554 (S11B-C) and when analysis is focused on tdTomato clusters alone (S11D-E). We
555 interrogated expression of specific SMC marker genes such as *Myh11* and *Cnn1* in
556 tdTomato lineage traced cells, where we observe that downregulation of contractile
557 markers seen with *SMC-Adar1* KO is prevented with *Mda5* KO (S11F-G), indicating this
558 effect is due to activation of MDA5. *Findmarker* differential gene expression analysis
559 and heatmap visualization of marker genes from the three genotypes show near
560 identical patterns between control and *SMC-Adar1*$^{-/-}$*, Mda5*$^{-/-}$ mice (S11H)(*Findmarker*

561 analysis in Table S4). These data demonstrate most effect of *SMC-Adar1* KO is
562 secondary to MDA5 activation. A small gene set where expression is observed to be
563 downregulated in both *SMC-Adar1*$^{-/-}$ and *SMC-Adar1*$^{-/-}$*, Mda5*$^{-/-}$ mice compared to
564 control (S11H), suggesting that a small fraction of genes may be downregulated with
565 loss of SMC Adar1 RNA editing independent of MDA5. A second set of genes appear to
566 be downregulated with *SMC-Adar1*$^{-/-}$ however are increased with *SMC-Adar1*$^{-/-}$*, Mda5*$^{-/-}$
567 (S11H), suggesting a role for MDA5 in regulating the expression of these genes
568 independent of *Adar1*.
569
570 ***SMC specific haploinsufficiency of Adar1 activates the ISG response in***
571 ***atherosclerosis and increases vascular chondromyoctye formation***
572 Although conditional homozygous deletion of *Adar1* in SMCs caused a profound and
573 rapid onset phenotype *in vivo* in a manner dependent on Mda5, we aimed to understand
574 if haploinsufficiency of *Adar1* in SMCs, where mice appear to have no discernable
575 phenotype, may lead to MDA5 activation, SMC phenotypic modulation, and progression
576 of atherosclerosis. To do this, we used the *SMC-Adar1*$^{-/+}$ (*Adar1*$^{fl/WT}$, *Myh11*^{CreERT2},
577 *ROSAtdTomato*, *ApoE*$^{-/-}$) mice with genotype controls (*Adar1*$^{WT/WT}$, *Myh11*^{CreERT2},
578 *ROSAtdTomato*, *ApoE*$^{-/-}$), dosed with tamoxifen at 7.5 weeks of age, and placed on high
579 fat diet for 16 weeks (Fig 5A). In this model, mice developed pronounced
580 atherosclerosis as we have shown previously[32,33,44,45]. *SMC-Adar1*$^{-/+}$ and control mice
581 had no differences in weight or lipid analysis (cholesterol, LDL, HDL, triglycerides) at
582 this 16-week timepoint (Fig S12). To understand the cellular resolution of the vessel
583 wall, at 16 weeks, we performed scRNAseq of the aortic root and ascending aorta. With
584 a total of 12 scRNAseq captures analyzing over 70,000 cells comparing *SMC-Adar1*$^{-/+}$
585 and control genotypes, we observed expected distinct cell clusters of SMCs, fibroblasts,
586 endothelial cells, macrophage cells, and T cells (Fig 5B). Lineage traced SMCs
587 demonstrated distinct SMC clusters as we have previously observed and have been
588 consistent with phenotypic modulation[33,44,45], with a mature SMC cluster, a fibromyocyte
589 (FMC) cluster, and a calcification promoting chondromyocyte (CMC) cluster of cells (Fig
590 5B). Importantly, *SMC-Adar1*$^{-/+}$ mice showed a large and distinct new SMC population
591 residing between the mature SMC population and the FMC population (Fig 5B).

592 Characterization of this population by *findmarker* analysis demonstrated this cluster to
593 express numerous markers of ISG activation (i.e. *Ifit3*, *Ifit1*, *Isg15*) consistent with MDA5
594 activation. Analysis of *Isg15* as a marker of ISG activation revealed notable expression
595 within this SMC cluster, termed 'SMC_ISG' (Fig 5B&C)(*Findmarker* results in Table S5).
596 To focus on the lineage traced SMC population, we performed an analysis on the
597 'SMC', 'SMC_ISG', 'FMC', and 'CMC' clusters. With subsequent dimensionality
598 reduction and repeat clustering, UMAP visualization highlighted the marked effect of
599 SMC *Adar1* haploinsufficiency in SMC phenotypic states in atherosclerosis (Fig 5D&E).
600 Top 10 marker genes and GO term enrichment for 'SMC', 'SMC_ISG', 'FMC', and
601 'CMC' clusters reveals the SMC_ISG cluster to be marked by ISGs including *Ifit3, Isg15,*
602 *Ifit1,* and *Irf7* and GO terms highlighting "response to virus", "response to interferon-
603 beta", and "defense response to virus" (Fig S13A&B). Evaluation of SMC marker *Myh11*
604 demonstrated downregulation of mature contractile markers with phenotypic modulation
605 (Fig S14A) with associated upregulation of FMC and CMC markers (i.e. *Tnfrsf11b*,
606 *Col2a1*, and *Acan*) (Fig S14B-D). Separation by genotype further highlighted that with
607 *SMC-Adar1*$^{-/+}$ mice, there was a shift away from mature SMCs, marked increase in the
608 SMC_ISG cluster (1.12% SMC_ISG in control vs 24.7% SMC_ISG in *SMC-Adar1*$^{-/+}$;
609 $p<E\text{-}100$), and an increase in CMC (16.3% CMC in control vs 22.6% CMC in *SMC-*
610 *Adar1*$^{-/+}$; $p=7.29E\text{-}100$)(Fig 5E&F). Comparison of the expression of CMC markers
611 *Col2a1* and *Acan* between genotypes demonstrated an increase in CMC cells with
612 *SMC-Adar1*$^{-/+}$ mice consistent with this finding (Fig S14E&F). This finding suggests that
613 ISG activation from SMC *Adar1* haploinsufficiency in atherosclerosis may be
614 contributing to CMC formation and vascular calcification.
615
616 ***Lineage trajectory analysis of vascular chondrogenesis reveals a distinct ISG***
617 ***dependent trajectory***
618 To investigate the potential for this SMC lineage relationship, we performed pseudotime
619 inference and cellular trajectory analysis with Slingshot[49]. By increasing clustering
620 resolution we generated 14 high resolution clusters of all tdTomato lineage traced
621 SMCs and performed Slingshot inference to understand the cellular trajectory between
622 mature SMC to CMC clusters. In this analysis, we observed only 2 distinct trajectories

623 between SMC and CMC (Fig 5H). Importantly, one trajectory excludes all SMC_ISG
624 clusters, while a second is dependent on SMC_ISG clusters (Fig 5H). This suggests two
625 distinct cellular trajectories to CMC formation, with one trajectory dependent on ISG
626 activation, while a second is ISG independent.

627 To better understand the top genes driving this ISG dependent trajectory, we
628 performed *findmarker* analysis on all high-resolution clusters and evaluated the top
629 markers for each cluster in sequence of the ISG dependent pathway (Fig S15A). This
630 analysis highlights that as SMC lose expression of contractile markers such as *Myh11*
631 and *Acta2*, they begin to express numerous ISGs. Initially, there is high expression of
632 *Irf7*, *Isg15*, *Ifit1*, which is then followed by increasing expression of *Ly6a*, *C3*, *Cxcl12*,
633 and other FMC markers such as *Dcn* and *Tnfrsf11b*, before SMCs have marked
634 expression of key CMC genes such as *Col2a1*, *Chad*, *Fmod*, and *Spp1* (Fig S15A). To
635 further understand the pathways driving this ISG dependent trajectory, we selected the
636 gene markers of the high-resolution clusters that are distinct to the ISG trajectory and
637 performed gene ontology pathway analysis (Fig S15B). Here, we identified top viral
638 immune response pathways including *'Coronavirus Disease'*, *'Influenza A'*, and
639 *'Epstein-Barr Virus infection'*, driven by genes such as *Jun, Ccl2*, *Il6*, *Nfkb1*, and this
640 analysis also reveals key JAK/STAT signaling molecules such as *Stat3* and *Jak1* (Fig
641 S15B). In addition to immune pathways, *'Focal Adhesion'* and *'Regulation of Actin*
642 *Cytoskeleton'* are highlighted, driven by genes such as *Rock1*, *Itgb1*, *Egfr,* PDGFs, and
643 *Map2k1*, suggesting a distinct interrelationship between activation of JAK/STAT and key
644 immune signaling pathways influencing focal adhesion pathways (Fig S15B).

645 To determine the location of MDA5 activation within the plaque and vessel wall,
646 we performed RNA scope on aortic root sections for *Isg15*. In control mice, we observed
647 scattered *Isg15* expression within the media, the base of the plaque and extending up to
648 the region beneath the cap, as well as in the adventitia (Fig 5I). However, in *SMC*
649 *Adar1*$^{-/+}$ mice we observed a marked increase in *Isg15* signal, with intense *Isg15*
650 expression within the media, throughout the plaque, and within the adventitia (Fig 5J).
651 Signal of *Isg15* RNAscope positive area in the vessel wall was quantified (Fig S16A)
652 and location of *Isg15* signal was compared to signal of chondromyocyte marker *Col2a1*,
653 where we reveal that cells that express *Isg15* reside in spatially distinct regions

654 compared to *Col2a1* (Fig S16B-C). These data suggest ISG activation in
655 atherosclerosis in control mice, however this effect is markedly increased with
656 haploinsufficiency of *Adar1* within the vascular SMC.
657
658 ***SMC specific haploinsufficiency in Adar1 increases plaque size and calcification***
659 ***in atherosclerosis***
660 We performed histological analysis of the aortic root for *SMC-Adar1*$^{-/+}$ and control
661 genotype mice after 16 weeks of high fat diet (n=13 each group). Using fluorescent
662 imaging of tdTomato and autofluorescence (elastin), we quantified plaque area and
663 plaque area normalized to total area of the internal elastic lamina area (IEL) (Fig 6A-D).
664 We observed that *SMC-Adar1*$^{-/+}$ mice had a significant increase in plaque area, an
665 effect that remained following normalization to overall area of the IEL (Fig 6A-D).
666 Notably, quantification of the area of the media (area between IEL and external elastic
667 lamina, EEL), we observed *SMC-Adar1*$^{-/+}$ mice to have a significant reduction, an effect
668 that remained following normalization to the total area of the EEL (Fig 6E&F). When
669 plaque area was normalized to media area, the observed effect with *SMC-Adar1*$^{-/+}$ mice
670 was further enhanced (Fig 6G). In addition, we observed total area of the EEL to be
671 increased (Fig 6H), suggesting an increased outward remodeling of the plaque. Given
672 our observation from single cell data that suggested increased chondromyocyte
673 formation, we evaluated the effect of SMC *Adar1* haploinsufficiency on calcification by
674 Ferangi Blue Chromogen staining (Fig 6I-L). We observed *SMC-Adar1*$^{-/+}$ mice to have a
675 significant increase in total Ferangi Blue staining by area (Fig 6K), an effect that
676 remained with normalization to plaque area (Fig 6L). These findings demonstrate that
677 SMC *Adar1* haploinsufficiency accelerate the formation atherosclerotic plaque area and
678 calcification.
679
680 ***SMC specific haploinsufficiency of Adar1 increased SMC lineage traced cell***
681 ***content in plaque without a change in acellular area***
682 Our data suggests that impaired RNA editing in vascular SMC leads to increased
683 plaque area and decreased media thickness, implicating increased SMC migration out
684 of the media and into the plaque. To investigate this, we quantified tdTomato positive

685 area within plaque as a marker of SMC lineage traced cells integrating into the plaque.
686 Here, we observed that in *SMC Adar1*$^{-/+}$ mice, the percent tdTomato area within plaque
687 is increased compared to control mice (p=0.0024)(Fig S17A-B). To then understand if
688 this increased SMC migration into the plaque results in a similar increase in tdTomato
689 area within the cap of the plaque, we measured the tdTomato area of the top 30μm
690 segment of the cap (Fig S17D). Here, we did not observe a significant difference,
691 although there was a greater mean tdTomato area in the SMC Adar1$^{-/+}$ mice
692 (p=0.0749).
693 To evaluate if there is increased acellular area within the plaque, we performed
694 Masson's Trichrome stains on lesions and quantified acellularity by tracing the plaque
695 and subtracting all area that has stain to then be able to quantify all acellular area. Here,
696 when normalizing acellular area by plaque area, we observed no difference between
697 genotypes (Fig S17E-G).
698
699 ***SMC specific haploinsufficiency in Adar1 has minimal effect on macrophage***
700 ***content in atherosclerosis***
701 With a subsetted analysis on all non-tdTomato lineage traced cell populations, we
702 observed that *SMC-Adar1*$^{-/+}$ mice have a small increase in total macrophage cell
703 populations in this 16-week atherosclerosis model (39.7% vs 35.2% of all non-tdTomato
704 cell population) (χ^2 *p=3.66E-26*) with minimal change in cell numbers across all other
705 cell types (Fig S18A&B). As we have shown that CCL signaling and Ccl5:Ccr5
706 appeared to be the dominant driver of macrophage recruitment in *SMC-Adar1*$^{-/-}$ mice,
707 we investigated if these signaling molecules were similarly upregulated in this 16-week
708 *SMC-Adar1*$^{-/+}$ atherosclerosis model. When performing receptor-ligand interaction
709 analysis using CellChat[47], we observed the 'SMC_ISG' cluster to have absent CCL
710 signaling and did not appear to act as a sender, receiver, mediator, or influencer (Fig
711 S18C&D). We then performed Cd68 immunohistochemical staining on aortic root
712 sections to evaluate for Cd68 positive area within the plaque between control and *SMC-*
713 *Adar1*$^{-/+}$ mice (Fig S18E-I). We observed that the total Cd68 positive area within the
714 plaque was significantly greater in the *SMC-Adar1*$^{-/+}$ mice (Fig S18G), however this
715 effect only trended towards significance when normalized to plaque area (Fig S18H) or

716 area of the total vessel at the internal elastic lamina (Fig S18I). The lack of a major
717 effect on macrophage content at this timepoint for this 16-week atherosclerosis *Adar1*
718 haploinsufficiency model is in contrast to our 2-week SMC-*Adar1* KO model (Fig 2) and
719 likely reflects a 'dose-dependent' response of SMC *Adar1* gene deletion, MDA5
720 activation, and *Ccl5* expression.
721
722 ***Haploinsufficiency of Mda5 prevents ISG activation and chondromyocyte***
723 ***formation in atherosclerosis with SMC-Adar1$^{-/+}$***
724 Homozygous as well as heterozygous deletion of *Mda5* (*Ifih1*) prevents mortality seen
725 with *SMC-Adar1* KO (Fig 3) and homozygous deletion of *Mda5* (*Ifih1*) prevents the
726 entirety of ISG activation in our single cell RNA sequencing analysis (Fig S11), raising
727 the question as to if deletion of *Mda5* can similarly prevent ISG induction and prevent
728 CMC formation observed with atherosclerosis with *SMC-Adar1* haploinsufficiency. To
729 investigate this, we further bred *SMC-Adar1$^{-/+}$* mice onto *Mda5* (*Ifih1*) heterozygous
730 background (*Adar1$^{fl/WT}$*, *Ifih1$^{-/+}$, Myh11^{CreERT2}*, *ROSAtdTomato*, *ApoE$^{-/-}$*) mice and
731 performed additional 16-week HFD atherosclerosis studies following tamoxifen dosing
732 at 7.5 weeks following our established protocol (Fig 5). We chose to use the *Mda5*
733 (*Ifih1*) heterozygous background over homozygous deletion given haploinsufficiency is
734 more akin to what may be achieved from future therapeutic inhibition. We performed
735 additional single cell RNA sequencing on the aortic root and ascending aorta with 9
736 mice for a total of 6 additional scRNAseq captures. Following data integration with a
737 total of more than 96K cells with >50,000 reads per cell (18 total scRNAseq libraries),
738 we evaluated how *Mda5* haploinsufficiency affects cellular phenotype and lineage
739 trajectory during atherosclerosis compared to control and *SMC-Adar1$^{-/+}$* genotypes. With
740 UMAP visualization, we demonstrate near identical overlap between the control and
741 *SMC-Adar1$^{-/+}$*, *Mda5$^{-/+}$* genotypes (Fig 7A), suggesting Mda5 haploinsufficiency to
742 largely prevent global transcriptomic effect of SMC *Adar1* haploinsufficiency. With
743 evaluation of key ISGs such as *Isg15*, we observe that *Mda5* haploinsufficiency
744 prevents the entirety of ISG induction (Fig 7B). With SMC subset analysis and
745 visualization of SMC clusters ('SMC', 'SMC_ISG', 'FMC', and 'CMC') we observe a clear
746 effect where *SMC-Adar1$^{-/+}$*, *Mda5$^{-/+}$* genotype eliminates the 'SMC_ISG' cluster seen

747 with *SMC-Adar1*$^{-/+}$ mice (Fig 7C), with further reduction in CMC formation (Fig 7C).
748 Upon evaluation of key marks of SMC, SMC_ISG, FMC, and CMC populations, we
749 observe that *Mda5* haploinsufficiency decreases the expression of CMC markers such
750 as *Col2a1* and *Acan* (Fig 7D-E) with near elimination of expression of 'SMC_ISG'
751 marker *Isg15* (Fig 7F). In quantifying the proportion of cells that belong to each SMC
752 cluster in the control, *SMC-Adar1*$^{-/+}$, and *SMC-Adar1*$^{-/+}$, *Mda5*$^{-/+}$ genotypes, we observe
753 that the control and *SMC-Adar1*$^{-/+}$ genotypes have 17% and 24% CMCs whereas the
754 *SMC-Adar1*$^{-/+}$, *Mda5*$^{-/+}$ genotype significantly reduces this proportion to 12% (Fig 7G).
755 This significant reduction in CMC population in the *SMC-Adar1*$^{-/+}$, *Mda5*$^{-/+}$ genotype is
756 significantly lower than not only the *SMC-Adar1*$^{-/+}$ genotype, but also the control
757 genotype (Fig 7G). This may suggest that even in control genotype, Mda5 is being
758 activated and contributing to CMC formation. Differential *findmarker* gene expression
759 analysis in the tdTomato population and heatmap visualization shows most marker
760 genes increased in *SMC-Adar1*$^{-/+}$ genotype compared to control are further decreased
761 in the *SMC-Adar1*$^{-/+}$, *Mda5*$^{-/+}$ genotype, suggesting the gene expression effect is
762 dependent on Mda5 (Fig 7H). However, similar to our observation in the SMC *Adar1* KO
763 + *Mda5* KO study (Fig S11), a portion of genes appear to be regulated by Adar1
764 independent of Mda5 and similarly a portion of genes appear to be regulated by Mda5
765 independent of Adar1 (Fig 7H). Upon evaluation of top ISGs (ie. *Isg15*, *Ifit3*, *Irf7*, *Stat1*),
766 we observe a consistent pattern of increased expression in *SMC-Adar1*$^{-/+}$ genotype
767 compared to control which is then blocked in entirety with the *SMC-Adar1*$^{-/+}$, *Mda5*$^{-/+}$
768 genotype (Fig 7I). Importantly, when evaluating key markers of SMC phenotypic
769 transition and FMC/CMC formation (ie. *Spp1*, *Fn1*, *Tnfrsf11b*, *Dcn*) we see a baseline
770 moderate level of expression in the control group, a significant increase in the *SMC-*
771 *Adar1*$^{-/+}$ genotype, and then a decrease in expression to a level lower than the control in
772 the *SMC-Adar1*$^{-/+}$, *Mda5*$^{-/+}$ genotype (Fig 7J). This is strong evidence to suggest that
773 Mda5 is playing a significant role in regulating SMC phenotypic transition in
774 atherosclerosis even with genetically intact *Adar1* RNA editing, consistent with our
775 noted finding of increasing ISG activation with SMC phenotypic transition in both human
776 and mouse in atherosclerosis (Fig 1) and human genetics data.

777 We measured the overall expression of *Ifih1* (Mda5) across genotypes where
778 featureplot visualization and mean normalized expression values show a pattern of
779 increasing expression of *Ifih1* (Mda5) with *SMC-Adar1*$^{-/+}$ (1.5 fold increase for all cells,
780 3.6 fold increase for SMC) (Fig S19). We observed a 65% and 58% reduction in *Ifih1*
781 (Mda5) expression in *SMC-Adar1*$^{-/+}$, *Mda5*$^{-/+}$ genotype compared to control in all cells
782 and SMC subset respectively (Fig S19). This data suggests that Mda5
783 haploinsufficiency not only produces a ~50-60% reduction in expression but prevents an
784 upregulation seen with *SMC-Adar1*$^{-/+}$.
785
786 ***ISG expression correlates to markers of SMC phenotypic modulation, plaque***
787 ***vulnerability, and plaque calcification in large human atherosclerosis dataset***
788 ***(Athero-Express)***
789 Our group's prior work has revealed edQTLs that reduce ADAR1 RNA editing to
790 correlate with increased ISG activation in human atherosclerotic plaque[12], and our
791 current analysis of human scRNAseq datasets have suggested the vascular SMC to
792 have a unique requirement for ADAR1 RNA editing and that ISG activation in SMCs
793 occurs with SMC phenotypic modulation (Fig 1). Although our comprehensive human *in*
794 *vitro* and murine *in vivo* models suggest a novel mechanism where impaired ADAR1
795 editing leads to altered SMC phenotype driving increasing atherosclerosis and
796 calcification through activation of MDA5 in an 'axis' of ADAR1-dsRNA-MDA5, there
797 remains a question as to if this relationship between ISG activation, adverse plaque
798 phenotype, and atherosclerotic plaque calcification remains true in larger human
799 populations. To address this question, we utilized our unique human database of carotid
800 endarterectomy samples (Athero-Express) where 1093 patient samples underwent bulk
801 RNA sequencing and paired with detailed histological characterization of plaque and
802 clinical phenotypic information (Fig 8A)[50]. Here, we evaluated the expression of key
803 ISGs, markers of SMC phenotypic modulation/calcification, and related their expression
804 to plaque phenotype.
805 The patient demographics for this dataset has been previously reported[50], briefly,
806 the patients enrolled are predominantly male (75.3%), mean age is 68.4yrs, and the
807 majority of patients have had symptomatic carotid stenosis (43.2% with stroke, 24.2%

808 with transient ischemic attack, 17.3% with ocular symptoms) with only 15.3%
809 asymptomatic. We first evaluated the distribution of RNA expression for 7 key ISGs
810 identified from our prior scRNAseq datasets (*ISG15*, *IFIH1*, *IFIT3*, *IFI16*, *IFI27*, *IFI35*,
811 *IFI44L*). We revealed a significant distribution of expression ranging from very low to
812 quite elevated with a similar level of distribution between these 7 ISGs (i.e. *IFIH1* and
813 *ISG15*, Fig S20A-B). We evaluated the expression between men and women by
814 normalized patient density by RNA expression and show there is no difference in
815 expression between sexes (i.e. *IFIH1* and *ISG15*, Fig S20C-D). To understand the
816 relationship in expression between these ISGs, we performed correlation and heat map
817 analysis and showed an overall positive correlation between ISGs with an unanticipated
818 exception of *IFIT3*, where *IFIT3* expression showed a slight negative correlation to other
819 ISGs (Fig S20E).
820 To understand the relationship of ISG expression and CMC formation we
821 performed linear regression analysis between individual ISGs and CMC markers *LUM*
822 and *HAPLN* (Fig 8B-E). We observed a strong positive relationship between expression
823 of ISGs and *LUM* and *HAPLN*, where, for example, the expression of *ISG15* showed a
824 significant linear relationship to *LUM* with a beta of 0.44 (*P=3.19E-39*) (Fig 8B) with a
825 similar relationship to *HAPLN* (Fig 8C). When evaluating the linear regression P-value
826 and beta coefficient across each ISG, we observe *IFI16* to have the strongest
827 relationship to *LUM* while *IFIH1* to have the strongest relationship to *HAPLN* (Fig 8D&E)
828 with a consistent pattern of increasing ISGs to have a significant linear relationship to
829 CMC markers. There was a notable exception of *IFIT3* that had a weak yet significant
830 negative relationship to *LUM* and *HAPLN*, perhaps suggesting distinct biology for *IFIT3*
831 (Fig 8D&E).
832 Given this relationship of ISG expression to CMC markers, we aimed to
833 understand if ISG expression correlates to plaque histological phenotype. Following the
834 adjustment for co-variates including age, sex, year of surgery, HTN, DM2, smoking,
835 LDL-C, lipid lowering and anti-platelet therapies, eGFR, DMI, history of CVD (see
836 methods), we evaluated the correlation of ISG expression to overall plaque vulnerability
837 (0-5 score), plaque calcification, total SMC area within the plaque, and total
838 macrophage area within the plaque. We observed that expression of ISGs *IFIH1*,

839 *IFI44L*, and *IFIT3* had a significant positive relationship to plaque vulnerability (Fig 8F).
840 Notably, increasing expression of *IFIH1* was associated with increased vulnerability of
841 plaque with a p-value of significance of *9.71E-135* (Fig 8F). We observed a similar
842 positive relationship between expression of *IFIH1* and measure of plaque calcification
843 (*P=0.02*) and a trend of significance for *IFI44L* (*P=0.052*) (Fig 8G).
844 A notable observation from our *in vivo* data shows that MDA5 activation can lead
845 to ISG activation and SMC cell death in the SMC *Adar1* homozygous KO model with
846 macrophage recruitment into the vessel wall, whereas the SMC *Adar1* heterozygous
847 model in atherosclerosis can lead to increased SMC recruitment into plaque with
848 minimal effect on macrophage recruitment. To understand how ISG activation relates to
849 SMC and macrophage investment into plaque in human disease, we evaluated the
850 relationship of ISG expression and the overall SMC and macrophage area within
851 plaque. Intriguingly, we observed a significant negative relationship between ISG
852 expression and SMC investment into plaque, where increasing expression of *ISG15*,
853 *IFI35*, *IFI16*, and *IFI27* were each significantly associated with decreasing SMC plaque
854 area (i.e. *IFI16 P=2.6E-4*)(Fig 8H). Importantly, we found ISG expression to have little
855 relationship to macrophage area within plaque, however, we did observe a significant
856 negative relationship between *IFI44L* expression and macrophage area within plaque
857 (Fig S20F).
858 These data together show that ISG activation in human plaque correlates to
859 increasing SMC phenotypic modulation and CMC formation, increasing plaque
860 vulnerability and calcification, while leading to decreased SMC investment within plaque
861 with minimal effect on macrophage recruitment.
862
863 **DISCUSSION**
864 Both academic and industry leaders are leveraging the power of human genetics to
865 drive discovery in the goal to define causal disease biology[51]. The rapid pace of
866 identifying novel genomic loci that meet genome wide level significance for complex
867 disease has resulted in notable challenges of target prioritization within a locus[52], as
868 well as prioritization for therapeutic drug development[53]. However, the association of
869 edQTL and CAD risk, where impaired RNA editing increases CAD risk while increasing

870 ISG activation, implicates a common disease pathway that is largely dependent on one
871 gene product — MDA5. Strikingly, 20% of CAD risk loci examined colocalized with
872 edQTL loci[12]. With a new understanding of the genetic determinants of RNA editing and
873 dsRNA sensing as an underlying etiology of coronary artery disease and other
874 inflammatory disorders[12], there is a significant need to define how this mechanism
875 influences disease risk.
876 Here, we provide a crucial link between the human genetics that implicate RNA
877 editing and dsRNA sensing by MDA5 in atherosclerosis and the biological
878 underpinnings of this disease association. Analysis of human atherosclerotic plaque
879 scRNAseq data indicate a pattern where SMCs express immunogenic RNA at high
880 levels and that ISG activation — suggestive of MDA5 activation with inadequate RNA
881 editing — occurs with SMC phenotypic modulation in both human and mouse data. We
882 further show that deletion of SMC specific *Adar1* in adult mice results in loss of vascular
883 integrity and significant mortality due to activation of MDA5 (Figs 2 and 3). Further,
884 scRNAseq analysis of aortic tissue reveals distinct ISG activation and a complex
885 transcriptional response and inflammatory cell recruitment within the vessel wall (Fig 4),
886 an effect blocked in its near entirety with deletion of MDA5 (Fig S11). This highlights the
887 absolute requirement for *Adar1* within the vascular SMC, but its role appears to be
888 primarily to prevent dsRNA activation of MDA5. Importantly, in 16-week atherosclerosis
889 studies in *Adar1* haploinsufficient mice, scRNAseq reveals ISG activation in SMCs in a
890 cell type and context specific mechanism driving phenotypic modulation, vascular
891 chondromyocyte formation, and to a lesser extent macrophage recruitment (Fig 5), and
892 that this coincides with increased plaque area, decreased thickness of the media, and
893 increased calcification (Fig 6). This effect of ISG activation and chondromyocyte
894 formation in SMC *Adar1* haploinsufficiency is prevented with only haploinsufficiency of
895 Mda5, suggesting the importance of Mda5 in mediating this effect (Fig 7). To
896 corroborate this finding in human datasets, we utilized the Athero-Express cohort of
897 carotid endarterectomy samples where patient data with careful histological examination
898 are paired with bulk RNA sequencing in 1093 patients[50]. Impressively, ISG expression
899 are positively associated with increasing plaque vulnerability, increasing plaque

900 calcification, and decreased SMC investment into the plaque, likely indicative of ISG
901 activation contributing to SMC cell death within the plaque (Figs 8 & S20).
902 These findings highlight an important new concept, that the need for RNA editing
903 to evade MDA5 activation not only occurs in a cell type specific manner, but a cellular
904 context specific manner. Two prior studies have investigated the role of SMC *Adar1* in
905 haploinsufficiency in SMC phenotypic modulation, focused on carotid injury[42] and an
906 angiotensin II model of abdominal aortic aneurysm (AAA)[41]. In these reports, the
907 authors reported that loss of SMC Adar1 prevented phenotypic modulation, however no
908 investigation into potential MDA5 activation was performed. Our data reported here
909 appears in contrast to this finding, however our findings implicate that the effect of loss
910 of ADAR1 on phenotypic transition is dependent on MDA5 activation and occurs in a
911 'dose dependent' mechanism where increasing MDA5 activation has a greater effect. In
912 the SMC *Adar1*$^{-/+}$ model, there is no immediate activation of MDA5, however in specific
913 cellular contexts immunogenic RNA formation appears to 'max out' the RNA editing
914 capacity of the single *Adar1* allele leading to MDA5 activation. This effect is overt in a
915 16-week high fat diet model of atherosclerosis; however, this was perhaps not evident in
916 either of the prior short term carotid injury or AAA models. However, a recent discovery
917 that MDA5 (*IFIH1*) is a locus in a large GWAS of AAA raises an intriguing hypothesis
918 that ADAR1 and MDA5 are causal mechanisms in AAA formation[54].
919 Our data indicate that SMC phenotypic modulation is a cellular context that
920 requires heightened RNA editing and that deficient RNA editing with SMC *Adar1*
921 heterozygous mice leads to MDA5 activation that accelerates SMC phenotypic changes
922 and disease state. Although our data suggests that expression of *ADAR1* increases
923 slightly with SMC phenotypic modulation *in vitro* and in atherosclerosis (Figs S1 and
924 S5), this likely reflects inadequate compensatory response leading to an overall
925 accumulation of dsRNA and MDA5 activation in specific cell states, influencing SMC
926 phenotype. These data reveal trajectories to SMC formation of the vascular
927 chondromyocyte (CMC), where ISG activation through MDA5 facilitates the formation of
928 CMCs and vascular calcification. This effect of MDA5 activation on SMC phenotypic
929 state is consistent with prior work investigating the role of ADAR1 and MDA5 on cellular
930 proliferation and cell death[13]. ADAR1, through its role of editing dsRNA and preventing

931 MDA5 activation, is crucial in regulating proliferation and deterring endogenous dsRNA
932 from triggering transcriptional shutdown and apoptotic cell death through activation of
933 PKR (*EIF2AK2*)[13]. It was previously reported that with initial KD of *ADAR1*, cell
934 proliferation was found to be increased, however with mounting MDA5 activation there
935 was ultimately PKR activation and transcriptional shut down and cell death[13]. This
936 effect, where initial loss of ADAR1 stimulates proliferation and cell state transitions, is
937 perhaps consistent with modifying a cell state similar to SMC to FMC transition in
938 atherosclerosis in our SMC *Adar1*$^{-/+}$ model. However, with overwhelming MDA5
939 activation as seen in our SMC *Adar1*$^{-/-}$ model, there is transcriptional shut down, cell
940 death, and major vascular effect. This biology may explain why in our human
941 atherosclerosis dataset ISG expression was associated with decreasing SMC
942 investment into plaque (Fig 8). This is somewhat in contrast to our *in vivo* SMC *Adar1*$^{-/+}$
943 model of atherosclerosis where we see ISG activation leading to increased SMC
944 migration into the plaque, however this may reflect the countering biology where overt
945 ISG activation can precipitate cell death and plaque instability.
946 Importantly, although classical inflammatory mechanisms have been implicated
947 in the pathogenesis of atherosclerosis and tremendous interest has been placed in the
948 potential to inhibit these pathways to treat disease[55], only a small minority of GWAS loci
949 in CAD implicate inflammatory pathways[2-5]. This finding raises the question as to the
950 overall weight of effect for disease causality for such inflammatory mediators (i.e. IL6,
951 TNFα, and IL1β). The relatively minimal benefit of IL1β antagonism in CAD[56] may
952 suggest an overall limited potential to treat disease through inhibition of these
953 inflammatory mediators. However, dsRNA sensing by MDA5 and ISG activation as an
954 overarching mechanism provides a new avenue of understanding as to how
955 inflammatory mechanisms are driving disease biology. Our data demonstrates that ISG
956 activation occurs in SMCs during atherogenesis, however the exact function of these
957 ISGs remains unclear. The function of ISGs has been previously reviewed[57], however,
958 ultimately IFN and ISGs serve key roles to regulate cellular viral immune response,
959 likely through driving transcriptional shutdown in a PKR dependent mechanism of cells
960 infected by a viral pathogen. Importantly, Type I interferon induces JAK/STAT
961 intracellular signaling pathways[57], a finding we observed in our ISG dependent cellular

962 trajectory in SMC phenotypic transition (Fig 5H & Fig S15). This finding suggests that
963 JAK/STAT is an important regulator of this trajectory. Specific ISGs have distinct roles in
964 fighting viral infection, for example on inhibiting viral entry (IFITM1/2/3), mRNA
965 synthesis (IFI16), protein synthesis (PKR), and mRNA degradation (ISG20)[57]. The
966 mechanism by which specific ISGs may modify atherosclerosis within the vessel wall
967 remains unclear. However, an important observation from human genetics is that
968 edQTL loci, which ultimately implicates dsRNA formation, MDA5 activation, and ISG
969 induction, to be a greater driver of disease heritability than all eQTLs in CAD[12]. This
970 data presented here further implicates a specific mechanism of disease while
971 highlighting a unique opportunity to leverage this biology for therapeutic development by
972 prioritizing the inhibition of dsRNA sensing and downstream activation of MDA5.
973

974 **MATERIALS AND METHODS**

975 **Data availability**

976 All raw and processed sequencing data are deposited in the National Center for
977 Biotechnology Information Gene Expression Omnibus. Bulk and single cell RNA
978 sequencing data is available through accession IDs GSE254862, GSE255661, and
979 GSE280641.
980

981 **Mouse Models**

982 To generate SMC-specific deletion of *Adar* we used the *Adar*$^{flox/flox}$ allele (exon 7-9
983 floxed; MGI allele: Adar$^{tm1.1Phs}$; MGI:3828307) as we have reported previously[58],
984 crossed onto the validated SMC-specific mouse Cre allele (*Myh11*^{CreERT2}) combined
985 with the floxed tandem dimer tomato (tdT) fluorescent reporter protein gene knocked
986 into the ROSA26 locus (B6.Cg-Gt(ROSA)26Sortm14(CAGtdTomato)Hze/J) and *ApoE*$^{-/-}$
987 alleles (*Adar*$^{flox/flox}$, *Myh11*^{CreERT2}, *ROSAtdT*/+, *ApoE*$^{-/-}$). To induce homozygous or
988 heterozygous deletion of *Adar1* in SMCs (*SMC-Adar1*$^{-/-}$: *Adar1*$^{fl/fl}$, *Myh11*^{CreERT2},
989 *ROSAtdTomato*, *ApoE*$^{-/-}$ or *SMC-Adar1*$^{-/+}$: *Adar1*$^{fl/WT}$, *Myh11*^{CreERT2}, *ROSAtdTomato*,
990 *ApoE*$^{-/-}$), mice receive 2 doses of tamoxifen (200mg/kg, P.O.) at 7.5-8 weeks of age
991 (dose 1 - day 0; and dose 2 - day 2) and started on a high fat diet as we have done
992 previously.[44,45] To evaluate the effect of MDA5 KO on *Adar1* KO background, we

993 crossed the *Ifih1*$^{-/-}$ mouse (B6.Cg-*Ifih1*$^{tm1.1Cln}$/J) that we have used previously[58], onto the
994 above background in a heterozygous manner to generate SMC *Adar1*$^{-/-}$ x Mda5$^{-/+}$ mice
995 (Adar$^{flox/flox}$, *Ifih1*$^{-/+}$, Myh11^{CreERT2}, ROSAtdT/+, ApoE$^{-/-}$), SMC *Adar1*$^{-/-}$ x Mda5$^{-/-}$ mice
996 (*Adar*$^{flox/flox}$, *Ifih1*$^{-/-}$, *Myh11*^{CreERT2}, *ROSAtdT*/+, *ApoE*$^{-/-}$), or SMC *Adar1*$^{-/+}$ x MDA5$^{-/+}$ mice
997 (*Adar*$^{flox/WT}$, *Ifih1*$^{-/+}$, *Myh11*^{CreERT2}, *ROSAtdT*/+, *ApoE*$^{-/-}$).
998
999 **Mouse aortic root/ascending aorta cell dissociation**
1000 Immediately after sacrifice, mice were perfused with phosphate buffered saline (PBS).
1001 The aortic root and ascending aorta were excised, up to the level of the brachiocephalic
1002 artery. Tissue was washed three times in PBS, placed into an enzymatic dissociation
1003 cocktail (2 U ml−1 Liberase (5401127001; Sigma–Aldrich) and 2 U ml−1 elastase
1004 (LS002279; Worthington) in Hank's Balanced Salt Solution (HBSS)) and incubated at 37
1005 °C for 45min, and subsequently minced. The cell suspension was further dissociated
1006 with 1ml pipette 20X and single cell suspension was confirmed under microscope. Cells
1007 were then pelleted by centrifugation at 500g for 5 min. The enzyme solution was then
1008 discarded, and cells were resuspended in fresh HBSS and passed through a 35um filter
1009 into a FACS tube. To increase biological replication, a single mouse was used to obtain
1010 single-cell suspension, and three mice were used in combination for each scRNA
1011 capture. 3 separate pairs of isolation were performed for control, *SMC-Adar1*$^{-/+}$, *SMC-*
1012 *Adar1*$^{-/-}$, *SMC-Adar1*$^{-/-}$, *Mda5*$^{-/-}$, or *SMC-Adar1*$^{-/+}$, *Mda5*$^{-/+}$ mice. Cells were FACS sorted
1013 based on tdTomato expression. tdT+ cells (considered to be of SMC lineage) and tdT−
1014 cells were then captured on separate but parallel runs of the same scRNA-Seq workflow
1015 (gating strategy and threshold identical to those published in previous work by Wirka et
1016 al[33]), and datasets were later combined for all subsequent analyses.
1017
1018 **Mouse aortic root histology**
1019 IHC was performed according to standard protocol. Primary antibodies for CD68 rabbit
1020 polyclonal antibody (1:400 dilution; ab125212; Abcam) with secondary rabbit-on-rodent
1021 HRP polymer (RMR622; BioCare Medical) for CD68 evaluation. Hematoxylin and eosin
1022 (H&E) and Trichrome staining was performed using standard protocols using and H&E
1023 and Trichrome Stain Kits (Abcam, ab245880 and ab150686 respectively). The

1024 processed sections were visualized using a Leica DM5500 microscope objective
1025 magnifications, and images were obtained using Leica Application Suite X software. For
1026 quantification of atherosclerosis plaque area, sections obtained at equal distance
1027 measured from the superior margin of the coronary sinus were used for comparison to
1028 ensure equal level sections were obtained. Images with FITC autofluorescence and
1029 tdTomato with red channel representing SMC lineage traced cells were obtained. Areas
1030 of interest were quantified using ImageJ (National Institutes of Health) software and
1031 compared using a two-sided t-test. Lesion size was defined by the area encompassing
1032 the intimal edge of the lesion to the border of SMC-marker positive intima-media
1033 junction. Calcification was evaluated using Ferangi Blue Chromogen Kit 2 (Biocare
1034 Medical, FB813) following manufacturers protocol. For RNAscope, slides were
1035 processed and hybridized according to the manufacturer's protocol, with reagents from
1036 ACD Bio. All area quantification was performed in a genotype blinded fashion with
1037 image J using length information embedded in exported files. All biological replicates for
1038 each staining were performed simultaneously on position-matched aortic root sections
1039 to limit intra-experimental variance.
1040
1041 **Single-cell capture and library preparation and sequencing**
1042 All single-cell capture and library preparation was performed in the Quertermous lab,
1043 sequencing was performed by Medgenome Inc (Foster City, CA). Cells were loaded into
1044 a 10x Genomics microfluidics chip and encapsulated with barcoded oligo-dT-containing
1045 gel beads using the 10x Genomics Chromium controller according to the manufacturer's
1046 instructions. Single-cell libraries were then constructed according to the manufacturer's
1047 instructions (Illumina). Libraries from individual samples were multiplexed into one lane
1048 before sequencing on an Illumina platform with targeted depth of 50,000 reads per cell
1049 for RNA or 400 million paired end reads per sequencing library.
1050
1051 **Analysis of scRNA-Seq data**
1052 Fastq files from each experimental time point and mouse genotype were aligned to the
1053 reference genome (mm10) individually using CellRanger Software (10x Genomics). The
1054 dataset was then analyzed using the R package Seurat 30[32] and datasets were merged

1055 in Seurat using standard Merge function. The dataset was trimmed of cells expressing
1056 fewer than 2000 genes, and genes expressed in fewer than 50 cells. The number of
1057 genes, number of unique molecular identifiers and percentage of mitochondrial genes
1058 were examined to identify outliers. As an unusually high number of genes can result
1059 from a 'doublet' event, in which two different cell types are captured together with the
1060 same barcoded bead, cells with >9000 genes were discarded. Cells containing >7.5%
1061 mitochondrial genes were presumed to be of poor quality and were also discarded. The
1062 gene expression values then underwent library-size normalization and normalized using
1063 established LogNormalize function in Seurat. No additional batch correction was
1064 performed. Principal component analysis was used for dimensionality reduction,
1065 followed by clustering in principal component analysis space using a graph-based
1066 clustering approach via Louvain algorithm. UMAP was then used for two-dimensional
1067 visualization of the resulting clusters. Pseudotime trajectory analysis was performed
1068 using Slingshot[49] with available software. Analysis, visualization and quantification of
1069 gene expression and generation of gene modulescores were performed using Seurat's
1070 built-in function such as "FeaturePlot", "VlnPlot", "AddModuleScore", and "FindMarker."
1071 Inference analysis of cell-cell communication was performed using CellChat[47]. Standard
1072 CellChat protocol was used where overexpressed genes, interactions, and
1073 communication probability was computed and subsequently aggregated and visualized
1074 across cell clusters.
1075 For immunogenic RNA score, we generated an AddModuleScore 'score' that
1076 summates the expression of all 'immunogenic' RNA from a putative list that was
1077 generated by combining our data from experimental *in vitro* models[27] along with human
1078 genetic edQTL analysis[12] and complete list of immunogenic RNA is included in Table
1079 S1.
1080
1081 **HCASMC culture and *in vitro* genomic studies**
1082 Cells were cultured in smooth muscle growth medium (Lonza; catalog number: CC-
1083 3182) supplemented with human epidermal growth factor, insulin, human basic
1084 fibroblast growth factor and 5% FBS, according to the manufacturer's instructions. All
1085 HCASMC lines were used at passages 4–8. HCASMCs immortalized with hTert

1086 transgene were acquired from Dr. Clint Miller (UVA) were used for all calcification
1087 assays with HCASMCs between passages 31 and 35. siRNA knockdowns were
1088 performed using Lipofectamine RNAiMax (Life Technologies) using manufacturer's
1089 recommended protocol at 50pg siRNA / 100,000cells.
1090
1091 **Phenotypic transition, calcification, and TGFβ assays**
1092 For phenotypic transition assays, HCASMC are cultured in 5% BSA and then subjected
1093 to serum starvation for 2 days. Following 2 days of serum starvation (0% BSA)
1094 HCASMCs develop a mature SMC phenotype, reintroduction of serum (5%) stimulates
1095 a more proliferative phenotype and RNA/protein is isolated 48hrs following
1096 reintroduction of serum. For calcification assays, HCASMCs are cultured in 1% BSA
1097 with 10mM beta-glycerophosphate and 8mM CaCl2 for 7 to 10 days. For TGFβ
1098 stimulation assays, we cultured HCASMC to confluency, treated with siRNA for 48
1099 hours, and transitioned cells to a serum free condition for 72 hours. We then stimulated
1100 cells with TGFβ (10ng/mL) or control for 72 hours before we isolated RNA and
1101 performed quantitative PCR.
1102
1103 **RNA isolation and Bulk RNA sequencing**
1104 RNA was isolated from disrupted HCASMC cells using standard RNeasy mini kit
1105 protocol (Qiagen). Isolated RNA underwent quality assessment, cDNA conversion, and
1106 library construction by Novogene (San Jose, CA). cDNA libraries were sequenced using
1107 Illumina Novoseq 6000 achieving 20-30 million paired-end reads per sample. RNAseq
1108 data were processed using a workflow starting from fastq files and code is available on
1109 github (https://github.com/zhaoshuoxp/Pipelines-Wrappers/blob/master/RNAseq.sh). In
1110 brief, the quality control was performed using FastQC, mapping to the human genome
1111 hg19/GRCh37 was performed using STAR second pass mapping to increase the
1112 percentage of mapped reads, and counting was done with featureCounts using
1113 GENCODE gtf annotation. Next, differential analysis was performed using DESeq2.
1114
1115 **RNA editing analysis**
1116

1117 RNA editing analysis in bulk RNA seq data was performed following a pipeline as we
1118 have done previously[12]. Briefly, we compiled a list of reference editing sites for
1119 quantification. By incorporating known sites in the RADAR database[59], tissue-specific
1120 sites identified in GTEx V6p17, and recently published hyper-editing sites[60], we finalized
1121 a list of 2,802,572 human editing sites. To quantify the editing levels, we computed the
1122 ratio of G reads divided by the sum of A and G reads at each site. Because the bulk
1123 RNA-seq data from HCASMC cells was not strand specific, the reads cannot be
1124 automatically assigned to sense and antisense strands, so that the quantification of
1125 editing level may be affected by expression of either of the two overlapping genes.
1126 Therefore, we developed a method to measure the RNA editing level of a given site
1127 using the reads derived from the corresponding transcript (sense for A-to-G edits and
1128 antisense for T-to-C edits), with less influence by the other overlapping transcript. For
1129 reads that are edited, they would be derived from the sense transcript if the edits are A-
1130 to-G, and from the antisense transcript if the edits are T-to-C. For the rest of the reads
1131 that are unedited, we estimated the numbers derived from the sense versus antisense
1132 transcripts in proportion to their expression levels. Overall RNA editing frequency was
1133 reported as percentage of total RNA editing sites across the genome.
1134

1135 **Athero-Express Bulk RNA isolation/sequencing and histological staining and**
1136 **analysis**

1137 Data from the Athero-Express Biobank study were used for the ISG expression
1138 validation in human carotid endarterectomy samples. The AE is an ongoing biobank
1139 study including endarterectomy patients from two tertiary hospitals in the Netherlands.
1140 Patients provided written informed consent, the medical ethics committee of the
1141 respective hospitals approved of the study (protocol number 22/018), and the study
1142 adheres to the Declaration of Helsinki[61]. A total of 1,093 plaque segments were selected
1143 from two subsequent experiments, Athero-Express RNA Study 1 and 2 (n = 622 and n =
1144 471, respectively). RNA was isolated using in-house standardized protocols. Library
1145 preparation utilized the CEL-seq2 method. This method yielded the highest mappability
1146 reads to the annotated genes. It captures the 3' end of polyadenylated RNA species and
1147 includes unique molecular identifiers (UMIs), which allows for direct counting of the

1148 unique RNA molecules. This plaque sample processing for RNA isolation and library
1149 preparation has previously been described in detail[50]. Both AERNAS1 and AERNAS2
1150 where mapped against the cDNA reference of all transcripts in GRCh38.p13 and
1151 Ensembl 108 (GRCh38.p13/ENSEMBL_GENES_108). These include raw read counts
1152 of all non-ribosomal, protein coding genes with existing HGNC gene name. All read
1153 counts are corrected for UMI sampling by `raw.genecounts=round(-4096*(log(1-
1154 (raw.genecounts/4096))))`.

1155 For histological analysis, stained slides are digitally stored up to 40X
1156 magnification. Semi-quantitatively scoring was performed by two independent
1157 observers, and a third independent observer if interpretations between the first two
1158 differed. Multiple stains were used to phenotype each plaque segment. Collagen
1159 content was assessed using picrosirius red and elastin von Gieson staining. Smooth
1160 muscle cells were identified using alpha actin, and macrophages using CD68 staining.
1161 Hematoxylin–Eosin (H&E) staining was used to evaluate calcification and the lipid core.
1162 In combination with Fibrin (Mallory's phosphotungstic acid-hematoxylin), H&E was also
1163 used to detect the presence of intraplaque haemorrhage (IPH). The scoring protocol of
1164 the semi quantitative scoring has been described previously[61,62]. The alpha actin
1165 (smooth muscle cell) and CD68 (macrophage) are also analysed quantitatively by
1166 computerized analysis. To assess plaque vulnerability, we use the plaque vulnerability
1167 index (PVI), a histological score incorporating collagen, macrophages, smooth muscle
1168 cells, lipid content and intraplaque haemorrhage[61]. Each trait was scored as stable or
1169 unstable, yielding a cumulative vulnerability score from 0 to 5.

1170 The multivariable linear regression analyses between the ISG Expression and
1171 plaque characteristics were performed in R (version 4.4.1) using the `lm()`function to fit
1172 a linear model. The bulk RNA-Seq counts of the ISG genes were transformed using
1173 variance stabilization transformation. For each ISG gene and phenotype (smooth
1174 muscle cells, macrophages, calcification, and plaque vulnerability index), we modelled
1175 the gene expression against the phenotype and corrected for age, gender,
1176 hypertension, diabetes and smoker status, LDL cholesterol levels, use of lipid-lowering
1177 drugs, use of antiplatelets drugs, estimated glomerular filtration rate based on the
1178 MDRD formula, body mass index, history of cardiovascular diseases, level of stenosis,

and year of surgery. For the linear regression analysis between the ISG expression and CMC markers (*LUM & HAPLN*). The bulk RNA-Seq counts of both the ISG genes and CMC markers were transformed using variance stabilization transformation. We modelled each ISG gene against both CMC markers and corrected for Age, Sex and Year of surgery.

List of Supplementary Materials

Supplemental Figures

- Supplemental Figure 1. *SMC ADAR1 and MDA5 expression in atherosclerosis in mice*
- Supplemental Figure 2. *ADAR1 regulates RNA editing in human coronary SMCs and RNA editing requirement is dependent on cell context.*
- Supplemental Figure 3. *Loss of ADAR1 in human coronary artery SMCs (HCASMCs) regulates viral sensing transcriptomic response in vitro*
- Supplemental Figure 4. Global RNA editing is decreased in HCASMC following phenotypic modulation in vitro
- Supplemental Figure 5. *Serum and TGFβ stimulation upregulate ADAR1 expression with differential effect on ISG induction in HCASMC.*
- Supplemental Figure 6. *Loss of ADAR1 regulates transcriptomic and inflammatory response to calcification in vitro*
- Supplemental Figure 7. *Quantification of histological findings for control and SMC-Adar1 KO mice*
- Supplemental Figure 8. *Aortas from SMC Adar1 KO with Mda5 KO are indistinguishable from control*
- Supplemental Figure 9. *SMC Adar1 KD induces antiviral defense transcriptional pathways*
- Supplemental Figure 10. *Loss of SMC Adar1 coordinates distinct response throughout vessel wall*
- Supplemental Figure 11. *Homozygous deletion of MDA5 (Ifih1) prevents transcriptomic effect of SMC-Adar1 KO*
- Supplemental Figure 12. *SMC Adar1 haploinsufficiency has no effect on weight or cholesterol in atherosclerosis high fat diet model*
- Supplemental Figure 13. *SMC specific haploinsufficiency of Adar1 in SMC subset analysis shows ISG activation with phenotypic modulation in atherosclerosis*
- Supplemental Figure 14. *SMC specific haploinsufficiency of Adar1 increases vascular chondromyoctye formation*
- Supplemental Figure 15. ISG dependent trajectory analysis from SMC to CMC implicates distinct gene ontologies
- Supplemental Figure 16. *Isg15 RNAscope reveals increased Isg15 signal in plaque of SMC Adar1$^{-/+}$ mice*

1221 • Supplemental Figure 17. *SMC specific haploinsufficiency in Adar1 increased*
1222 *SMC lineage traced cell content in plaque without change in acellular area*
1223 • Supplemental Figure 18. *SMC specific haploinsufficiency of Adar1 has minimal*
1224 *effect on macrophage infiltration in atherosclerosis*
1225 • Supplemental Figure 19. *Mda5 haploinsufficiency reduces Mda5 expression and*
1226 *prevents upregulation in SMC Adar1 het background.*
1227 • Supplemental Figure 20. *Variability of ISG expression between patient carotid*
1228 *endarterectomy samples with no difference between sexes in Athero-Express*
1229 *cohort.*
1230

1231

1232 **References**

1233

1234 1 Diseases, G. B. D. & Injuries, C. Global burden of 369 diseases and injuries in
1235 204 countries and territories, 1990-2019: a systematic analysis for the Global
1236 Burden of Disease Study 2019. *Lancet* **396**, 1204-1222 (2020).
1237 https://doi.org/10.1016/S0140-6736(20)30925-9
1238 2 Nikpay, M. *et al.* A comprehensive 1,000 Genomes-based genome-wide
1239 association meta-analysis of coronary artery disease. *Nat Genet* **47**, 1121-1130
1240 (2015). https://doi.org/10.1038/ng.3396
1241 3 Schunkert, H. *et al.* Large-scale association analysis identifies 13 new
1242 susceptibility loci for coronary artery disease. *Nat Genet* **43**, 333-338 (2011).
1243 https://doi.org/10.1038/ng.784
1244 4 van der Harst, P. & Verweij, N. Identification of 64 Novel Genetic Loci Provides an
1245 Expanded View on the Genetic Architecture of Coronary Artery Disease. *Circ Res*
1246 **122**, 433-443 (2018). https://doi.org/10.1161/CIRCRESAHA.117.312086
1247 5 Tcheandjieu, C. *et al.* Large-scale genome-wide association study of coronary
1248 artery disease in genetically diverse populations. *Nat Med* **28**, 1679-1692 (2022).
1249 https://doi.org/10.1038/s41591-022-01891-3
1250 6 Albert, F. W. & Kruglyak, L. The role of regulatory variation in complex traits and
1251 disease. *Nat Rev Genet* **16**, 197-212 (2015). https://doi.org/10.1038/nrg3891
1252 7 Consortium, G. T. The GTEx Consortium atlas of genetic regulatory effects
1253 across human tissues. *Science* **369**, 1318-1330 (2020).
1254 https://doi.org/10.1126/science.aaz1776
1255 8 Eisenberg, E. & Levanon, E. Y. A-to-I RNA editing - immune protector and
1256 transcriptome diversifier. *Nat Rev Genet* **19**, 473-490 (2018).
1257 https://doi.org/10.1038/s41576-018-0006-1
1258 9 Jonkhout, N. *et al.* The RNA modification landscape in human disease. *RNA* **23**,
1259 1754-1769 (2017). https://doi.org/10.1261/rna.063503.117
1260 10 Walkley, C. R. & Li, J. B. Rewriting the transcriptome: adenosine-to-inosine RNA
1261 editing by ADARs. *Genome Biol* **18**, 205 (2017). https://doi.org/10.1186/s13059-
1262 017-1347-3

1263 11 Gatsiou, A. & Stellos, K. RNA modifications in cardiovascular health and disease.
1264 *Nat Rev Cardiol* **20**, 325-346 (2023). https://doi.org/10.1038/s41569-022-00804-8
1265 12 Li, Q. *et al.* RNA editing underlies genetic risk of common inflammatory diseases.
1266 *Nature* **608**, 569-577 (2022). https://doi.org/10.1038/s41586-022-05052-x
1267 13 Chung, H. *et al.* Human ADAR1 Prevents Endogenous RNA from Triggering
1268 Translational Shutdown. *Cell* **172**, 811-824 e814 (2018).
1269 https://doi.org/10.1016/j.cell.2017.12.038
1270 14 Liddicoat, B. J. *et al.* RNA editing by ADAR1 prevents MDA5 sensing of
1271 endogenous dsRNA as nonself. *Science* **349**, 1115-1120 (2015).
1272 https://doi.org/10.1126/science.aac7049
1273 15 Goubau, D., Deddouche, S. & Reis e Sousa, C. Cytosolic sensing of viruses.
1274 *Immunity* **38**, 855-869 (2013). https://doi.org/10.1016/j.immuni.2013.05.007
1275 16 Chalk, A. M., Taylor, S., Heraud-Farlow, J. E. & Walkley, C. R. The majority of A-
1276 to-I RNA editing is not required for mammalian homeostasis. *Genome Biol* **20**,
1277 268 (2019). https://doi.org/10.1186/s13059-019-1873-2
1278 17 Nishikura, K. Functions and regulation of RNA editing by ADAR deaminases.
1279 *Annual review of biochemistry* **79**, 321-349 (2010).
1280 https://doi.org/10.1146/annurev-biochem-060208-105251
1281 18 Jain, M. *et al.* RNA editing of Filamin A pre-mRNA regulates vascular contraction
1282 and diastolic blood pressure. *EMBO J* **37** (2018).
1283 https://doi.org/10.15252/embj.201694813
1284 19 Pestal, K. *et al.* Isoforms of RNA-Editing Enzyme ADAR1 Independently Control
1285 Nucleic Acid Sensor MDA5-Driven Autoimmunity and Multi-organ Development.
1286 *Immunity* **43**, 933-944 (2015). https://doi.org/10.1016/j.immuni.2015.11.001
1287 20 Mannion, N. M. *et al.* The RNA-editing enzyme ADAR1 controls innate immune
1288 responses to RNA. *Cell reports* **9**, 1482-1494 (2014).
1289 https://doi.org/10.1016/j.celrep.2014.10.041
1290 21 Feigenbaum, A. *et al.* Singleton-Merten syndrome: an autosomal dominant
1291 disorder with variable expression. *Am J Med Genet A* **161A**, 360-370 (2013).
1292 https://doi.org/10.1002/ajmg.a.35732

1293 22 Rutsch, F., Buers, I. & Nitschke, Y. Hereditary Disorders of Cardiovascular
1294 Calcification. *Arterioscler Thromb Vasc Biol* **41**, 35-47 (2021).
1295 https://doi.org/10.1161/ATVBAHA.120.315577
1296 23 Stellos, K. *et al.* Adenosine-to-inosine RNA editing controls cathepsin S
1297 expression in atherosclerosis by enabling HuR-mediated post-transcriptional
1298 regulation. *Nat Med* **22**, 1140-1150 (2016). https://doi.org/10.1038/nm.4172
1299 24 Vlachogiannis, N. I. *et al.* Adenosine-to-inosine Alu RNA editing controls the
1300 stability of the pro-inflammatory long noncoding RNA NEAT1 in atherosclerotic
1301 cardiovascular disease. *J Mol Cell Cardiol* **160**, 111-120 (2021).
1302 https://doi.org/10.1016/j.yjmcc.2021.07.005
1303 25 Emdin, C. A. *et al.* Analysis of predicted loss-of-function variants in UK Biobank
1304 identifies variants protective for disease. *Nat Commun* **9**, 1613 (2018).
1305 https://doi.org/10.1038/s41467-018-03911-8
1306 26 Dias Junior, A. G., Sampaio, N. G. & Rehwinkel, J. A Balancing Act: MDA5 in
1307 Antiviral Immunity and Autoinflammation. *Trends Microbiol* **27**, 75-85 (2019).
1308 https://doi.org/10.1016/j.tim.2018.08.007
1309 27 Sun, T. *et al.* A Small Subset of Cytosolic dsRNAs Must Be Edited by ADAR1 to
1310 Evade MDA5-Mediated Autoimmunity. *bioRxiv*, 2022.2008.2029.505707 (2022).
1311 https://doi.org/10.1101/2022.08.29.505707
1312 28 Alsaigh, T., Evans, D., Frankel, D. & Torkamani, A. Decoding the transcriptome of
1313 calcified atherosclerotic plaque at single-cell resolution. *Commun Biol* **5**, 1084
1314 (2022). https://doi.org/10.1038/s42003-022-04056-7
1315 29 Alexander, M. R. & Owens, G. K. Epigenetic control of smooth muscle cell
1316 differentiation and phenotypic switching in vascular development and disease.
1317 *Annu Rev Physiol* **74**, 13-40 (2012). https://doi.org/10.1146/annurev-physiol-
1318 012110-142315
1319 30 Basatemur, G. L., Jorgensen, H. F., Clarke, M. C. H., Bennett, M. R. & Mallat, Z.
1320 Vascular smooth muscle cells in atherosclerosis. *Nat Rev Cardiol* **16**, 727-744
1321 (2019). https://doi.org/10.1038/s41569-019-0227-9
1322 31 Cheng, P. *et al.* ZEB2 Shapes the Epigenetic Landscape of Atherosclerosis.
1323 *Circulation* (2022). https://doi.org/10.1161/CIRCULATIONAHA.121.057789

1324 32 Kim, J. B. *et al.* Environment-Sensing Aryl Hydrocarbon Receptor Inhibits the
1325 Chondrogenic Fate of Modulated Smooth Muscle Cells in Atherosclerotic
1326 Lesions. *Circulation* **142**, 575-590 (2020).
1327 https://doi.org/10.1161/CIRCULATIONAHA.120.045981
1328 33 Wirka, R. C. *et al.* Atheroprotective roles of smooth muscle cell phenotypic
1329 modulation and the TCF21 disease gene as revealed by single-cell analysis. *Nat*
1330 *Med* **25**, 1280-1289 (2019). https://doi.org/10.1038/s41591-019-0512-5
1331 34 Cheng, P. *et al.* Smad3 regulates smooth muscle cell fate and mediates adverse
1332 remodeling and calcification of the atherosclerotic plaque. *Nature Cardiovascular*
1333 *Research* **1**, 322-333 (2022). https://doi.org/10.1038/s44161-022-00042-8
1334 35 Kim, H. J. *et al.* Molecular mechanisms of coronary artery disease risk at the
1335 PDGFD locus. *Nat Commun* **14**, 847 (2023). https://doi.org/10.1038/s41467-023-
1336 36518-9
1337 36 Sharma, D. *et al.* Comprehensive Integration of Multiple Single-Cell
1338 Transcriptomic Data Sets Defines Distinct Cell Populations and Their Phenotypic
1339 Changes in Murine Atherosclerosis. *Arterioscler Thromb Vasc Biol* **44**, 391-408
1340 (2024). https://doi.org/10.1161/ATVBAHA.123.320030
1341 37 Ramaswami, G. *et al.* Accurate identification of human Alu and non-Alu RNA
1342 editing sites. *Nat Methods* **9**, 579-581 (2012). https://doi.org/10.1038/nmeth.1982
1343 38 Shankman, L. S. *et al.* KLF4-dependent phenotypic modulation of smooth muscle
1344 cells has a key role in atherosclerotic plaque pathogenesis. *Nat Med* **21**, 628-637
1345 (2015). https://doi.org/10.1038/nm.3866
1346 39 Maurano, M. *et al.* Protein kinase R and the integrated stress response drive
1347 immunopathology caused by mutations in the RNA deaminase ADAR1. *Immunity*
1348 **54**, 1948-1960 e1945 (2021). https://doi.org/10.1016/j.immuni.2021.07.001
1349 40 Wong, D. *et al.* FHL5 Controls Vascular Disease-Associated Gene Programs in
1350 Smooth Muscle Cells. *Circ Res* **132**, 1144-1161 (2023).
1351 https://doi.org/10.1161/CIRCRESAHA.122.321692
1352 41 Cai, D. *et al.* A Novel Mechanism Underlying Inflammatory Smooth Muscle
1353 Phenotype in Abdominal Aortic Aneurysm. *Circ Res* **129**, e202-e214 (2021).
1354 https://doi.org/10.1161/CIRCRESAHA.121.319374

1355 42 Fei, J., Cui, X. B., Wang, J. N., Dong, K. & Chen, S. Y. ADAR1-Mediated RNA
1356 Editing, A Novel Mechanism Controlling Phenotypic Modulation of Vascular
1357 Smooth Muscle Cells. *Circ Res* **119**, 463-469 (2016).
1358 https://doi.org/10.1161/CIRCRESAHA.116.309003
1359 43 Cai, D. & Chen, S. Y. ADAR1 Is Essential for Smooth Muscle Homeostasis and
1360 Vascular Integrity. *Cells* **13** (2024). https://doi.org/10.3390/cells13151257
1361 44 Cheng, P. *et al.* Smad3 regulates smooth muscle cell fate and mediates adverse
1362 remodeling and calcification of the atherosclerotic plaque. *Nat Cardiovasc Res* **1**,
1363 322-333 (2022). https://doi.org/10.1038/s44161-022-00042-8
1364 45 Cheng, P. *et al.* ZEB2 Shapes the Epigenetic Landscape of Atherosclerosis.
1365 *Circulation* **145**, 469-485 (2022).
1366 https://doi.org/10.1161/CIRCULATIONAHA.121.057789
1367 46 Lendahl, U., Muhl, L. & Betsholtz, C. Identification, discrimination and
1368 heterogeneity of fibroblasts. *Nat Commun* **13**, 3409 (2022).
1369 https://doi.org/10.1038/s41467-022-30633-9
1370 47 Jin, S. *et al.* Inference and analysis of cell-cell communication using CellChat.
1371 *Nat Commun* **12**, 1088 (2021). https://doi.org/10.1038/s41467-021-21246-9
1372 48 Tyner, J. W. *et al.* CCL5-CCR5 interaction provides antiapoptotic signals for
1373 macrophage survival during viral infection. *Nat Med* **11**, 1180-1187 (2005).
1374 https://doi.org/10.1038/nm1303
1375 49 Street, K. *et al.* Slingshot: cell lineage and pseudotime inference for single-cell
1376 transcriptomics. *BMC Genomics* **19**, 477 (2018). https://doi.org/10.1186/s12864-
1377 018-4772-0
1378 50 Mokry, M. *et al.* Transcriptomic-based clustering of human atherosclerotic
1379 plaques identifies subgroups with different underlying biology and clinical
1380 presentation. *Nat Cardiovasc Res* **1**, 1140-1155 (2022).
1381 https://doi.org/10.1038/s44161-022-00171-0
1382 51 Plenge, R. M., Scolnick, E. M. & Altshuler, D. Validating therapeutic targets
1383 through human genetics. *Nat Rev Drug Discov* **12**, 581-594 (2013).
1384 https://doi.org/10.1038/nrd4051

1385 52 Mountjoy, E. *et al.* An open approach to systematically prioritize causal variants
1386 and genes at all published human GWAS trait-associated loci. *Nat Genet* **53**,
1387 1527-1533 (2021). https://doi.org/10.1038/s41588-021-00945-5
1388 53 Estrada, K. *et al.* Identifying therapeutic drug targets using bidirectional effect
1389 genes. *Nat Commun* **12**, 2224 (2021). https://doi.org/10.1038/s41467-021-
1390 21843-8
1391 54 Roychowdhury, T. *et al.* Genome-wide association meta-analysis identifies risk
1392 loci for abdominal aortic aneurysm and highlights PCSK9 as a therapeutic target.
1393 *Nat Genet* **55**, 1831-1842 (2023). https://doi.org/10.1038/s41588-023-01510-y
1394 55 Soehnlein, O. & Libby, P. Targeting inflammation in atherosclerosis - from
1395 experimental insights to the clinic. *Nat Rev Drug Discov* **20**, 589-610 (2021).
1396 https://doi.org/10.1038/s41573-021-00198-1
1397 56 Ridker, P. M. *et al.* Antiinflammatory Therapy with Canakinumab for
1398 Atherosclerotic Disease. *N Engl J Med* **377**, 1119-1131 (2017).
1399 https://doi.org/10.1056/NEJMoa1707914
1400 57 Schoggins, J. W. Interferon-Stimulated Genes: What Do They All Do? *Annu Rev*
1401 *Virol* **6**, 567-584 (2019). https://doi.org/10.1146/annurev-virology-092818-015756
1402 58 Hu, S. B. *et al.* ADAR1p150 prevents MDA5 and PKR activation via distinct
1403 mechanisms to avert fatal autoinflammation. *Mol Cell* **83**, 3869-3884 e3867
1404 (2023). https://doi.org/10.1016/j.molcel.2023.09.018
1405 59 Ramaswami, G. & Li, J. B. RADAR: a rigorously annotated database of A-to-I
1406 RNA editing. *Nucleic Acids Res* **42**, D109-113 (2014).
1407 https://doi.org/10.1093/nar/gkt996
1408 60 Porath, H. T., Knisbacher, B. A., Eisenberg, E. & Levanon, E. Y. Massive A-to-I
1409 RNA editing is common across the Metazoa and correlates with dsRNA
1410 abundance. *Genome Biol* **18**, 185 (2017). https://doi.org/10.1186/s13059-017-
1411 1315-y
1412 61 Verhoeven, B. A. *et al.* Athero-express: differential atherosclerotic plaque
1413 expression of mRNA and protein in relation to cardiovascular events and patient
1414 characteristics. Rationale and design. *Eur J Epidemiol* **19**, 1127-1133 (2004).
1415 https://doi.org/10.1007/s10564-004-2304-6

62 Mekke, J. M. *et al.* The accumulation of erythrocytes quantified and visualized by Glycophorin C in carotid atherosclerotic plaque reflects intraplaque hemorrhage and pre-procedural neurological symptoms. *Sci Rep* **13**, 17104 (2023). https://doi.org/10.1038/s41598-023-43369-3

Acknowledgements

Funding:

National Institutes of Health grant F32HL160067 (CW)
National Institutes of Health grant L30HL159413 (CW)
National Institutes of Health grant K08HL167699 (CW)
National Institutes of Health grant K08HL153798 (PC)
National Institutes of Health grant R01HL134817 (TQ)
National Institutes of Health grant R01HL139478 (TQ)
National Institutes of Health grant R01HL156846 (TQ)
National Institutes of Health grant R01HL151535 (TQ)
National Institutes of Health grant R01HL145708 (TQ)
National Institutes of Health grant UM1 HG011972 (TQ)
National Institutes of Health grant R35GM144100 (JBL)
National Institutes of Health grant R01MH115080 (JBL)
National Institutes of Health grant R01GM102484 (JBL)
American Heart Association grant 20CDA35310303 (PC)
American Heart Association grant 23CDA1042900 (CW)
American Heart Association grant 23POST1018991 (WG).

Author Contributions

Conceptualization: C.W., Q.L., P.C., J.B.L., and T.Q.

Methodology: C.W., Q.L., J.M.

Investigation: C.W., Q.L., J.M., H.G., D.G., W.G., M.W., Q.Z., M.R., D.L., B.P., A.B., R.K., T.N., T.P., M.M., C.M., S.L.

Visualization: C.W.

Funding acquisition: C.W., J.B.L., T.Q.

Project administration: C.W., J.B.L., T.Q.

Supervision: J.B.L., T.Q.

Writing — original draft: C.W., J.B.L., T.Q.

Writing — review and editing: C.W., Q.L., J.B.L., T.Q.

Competing interests:

C.W. is a consultant for AiRNA Bio and Avidity Biosciences. T.Q. serves on the scientific advisory board for Amgen. J.B.L. is a co-founder of AIRNA Bio and a consultant for Risen Pharma. J.B.L. and Q.L. are named inventors of a provisional patent filed by Stanford University (serial no. 63/473,678), describing a method related to RNA editing. The other authors declare no competing interests.

Data and materials availability:

All raw and processed sequencing data are deposited in the National Center for Biotechnology Information Gene Expression Omnibus. Bulk and single cell RNA sequencing data is available through accession IDs GSE254862, GSE255661, and GSE280641.

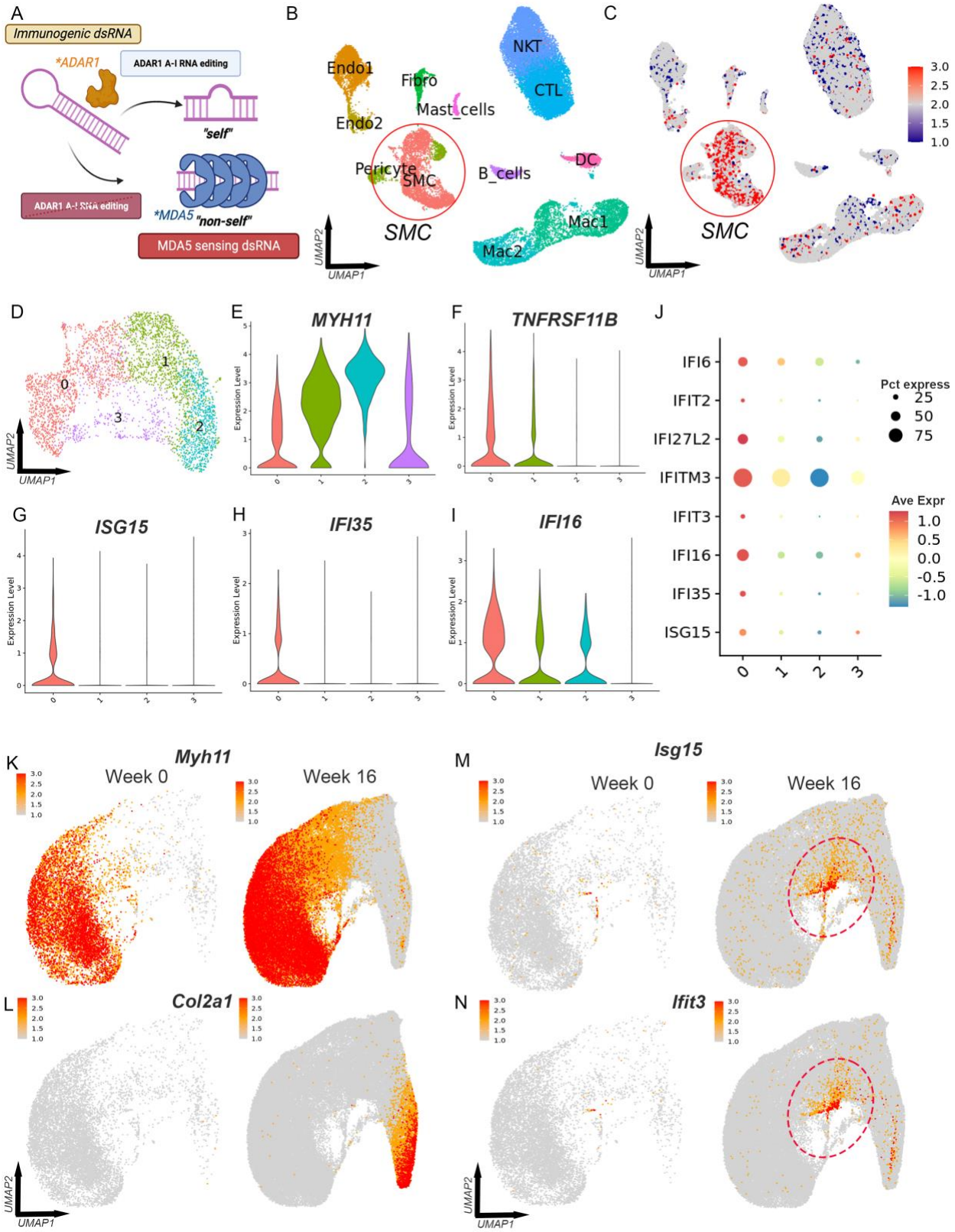

Figure 1. ***Smooth muscle cells in atherosclerosis express immunogenic RNA and show evidence of ISG induction in phenotypic modulation.*** (A) Schematic of

1472 ADAR1 RNA editing of dsRNA. (B) UMAP of scRNAseq data from human carotid
1473 atherosclerotic plaque (Alsaigh et al., 2022). (C) Module score of immunogenic RNA
1474 expression. (D) Clustering of SMC subset with (E) violin plot showing SMC marker
1475 *MYH11* with (F) fibromyocyte/chondromyocyte marker *TNFRSF11B*. (G-I) Violin plots of
1476 ISGs *ISG15* (G), *IF135* (H), and *IFI16* (I). (J) Dotplot of top ISGs within SMC clusters.
1477 (K-N) In mouse comprehensive integrated dataset of lineage traced SMCs (from
1478 Sharma et al., 2024), featureplot of *Myh11* (K) and *Col2a1* (L) at 0 and 16 weeks of high
1479 fat diet. (L-M) Featureplots of *Isg15* (L) and *Ifit3* (M) in SMC phenotypic modulation.
1480

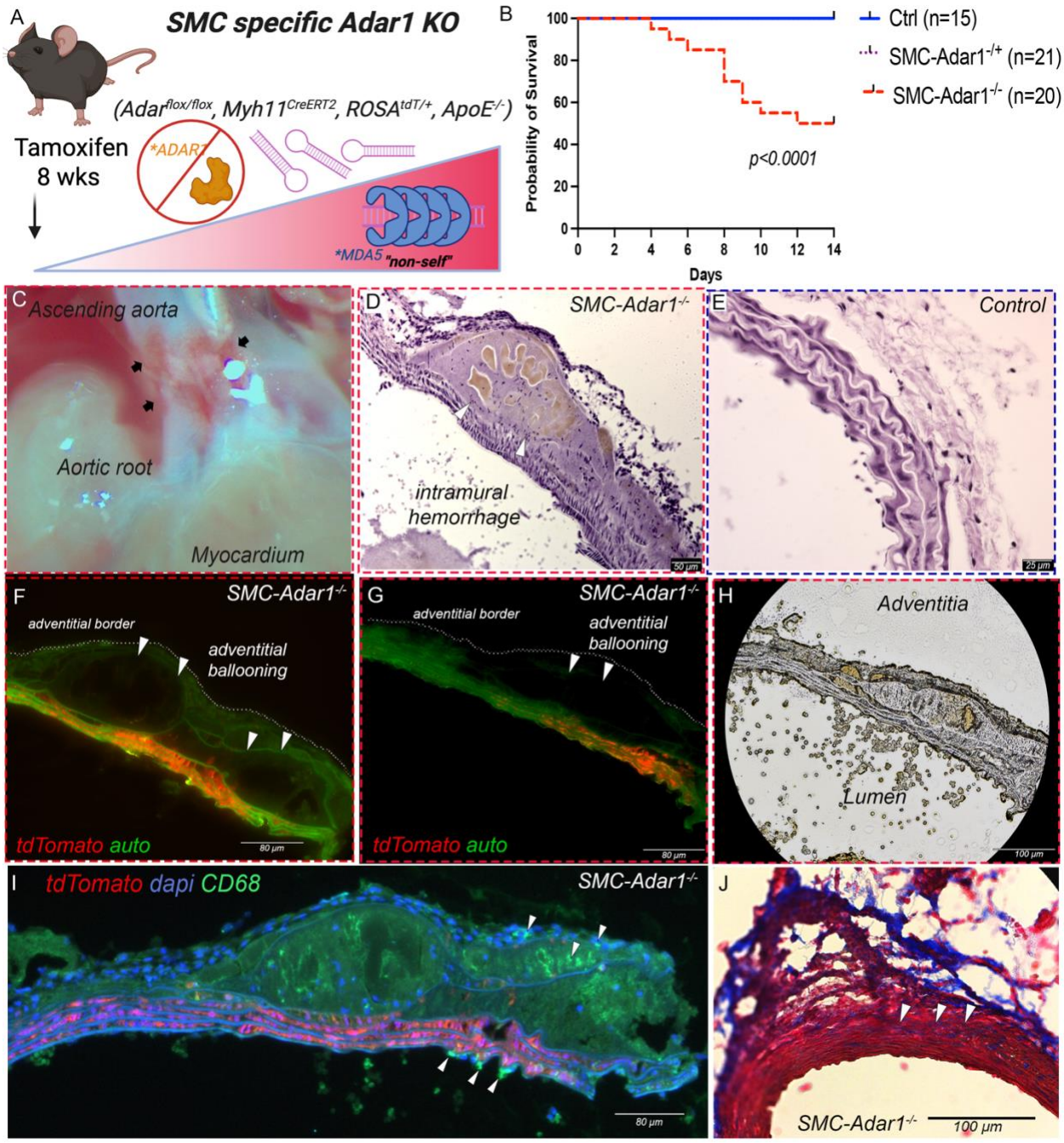

Figure 2*. SMC specific ADAR1 is required to maintain vascular integrity and survival.* (A) Schematic of SMC-*Adar1*$^{-/-}$ model and accumulation of dsRNA and MDA5 activation. (B) Survival curves for 56 mice treated with tamoxifen at 8 weeks of age, comparing *SMC-Adar1*$^{-/-}$, *SMC-Adar1*$^{-/+}$ (*Adar1*$^{fl/WT}$, *Myh11*^{CreERT2}, *ROSAtdTomato*, *ApoE*$^{-/-}$), and control (*Adar1*$^{WT/WT}$, *Myh11*^{CreERT2}, *ROSAtdTomato*, *ApoE*$^{-/-}$) genotypes. (C) Gross image of aortic root and ascending aorta of *SMC-Adar1*^{KO} mouse at 2 weeks

1488 following tamoxifen treatment. (D-E) Representative images of hematoxylin and eosin
1489 (H&E) staining from *SMC-Adar1*$^{-/-}$ (D) and control genotype mice (E). (F-G) Fluorescent
1490 imaging with autofluorescence indicating elastin (green) and Myh11 derived cells
1491 labeled with tdTomato (red) in two mice with adventitial ballooning in *SMC-Adar1*$^{-/-}$ (F-
1492 G). (H) Bright field imaging of aorta cross section from *SMC-Adar1*$^{-/-}$ mouse
1493 corresponding to fluorescent imaging in panel G. (I) Cd68 immunostaining of aorta
1494 cross section from *SMC-Adar1*$^{-/-}$ mouse showing macrophage infiltration. (J) Masson
1495 trichrome stain of aorta cross section from *SMC-Adar1*$^{-/-}$ mouse showing intra-medial
1496 collagen deposition. *P*-value represents comparison of survival curves, Log-rank
1497 (Mantel-Cox) test (B).
1498

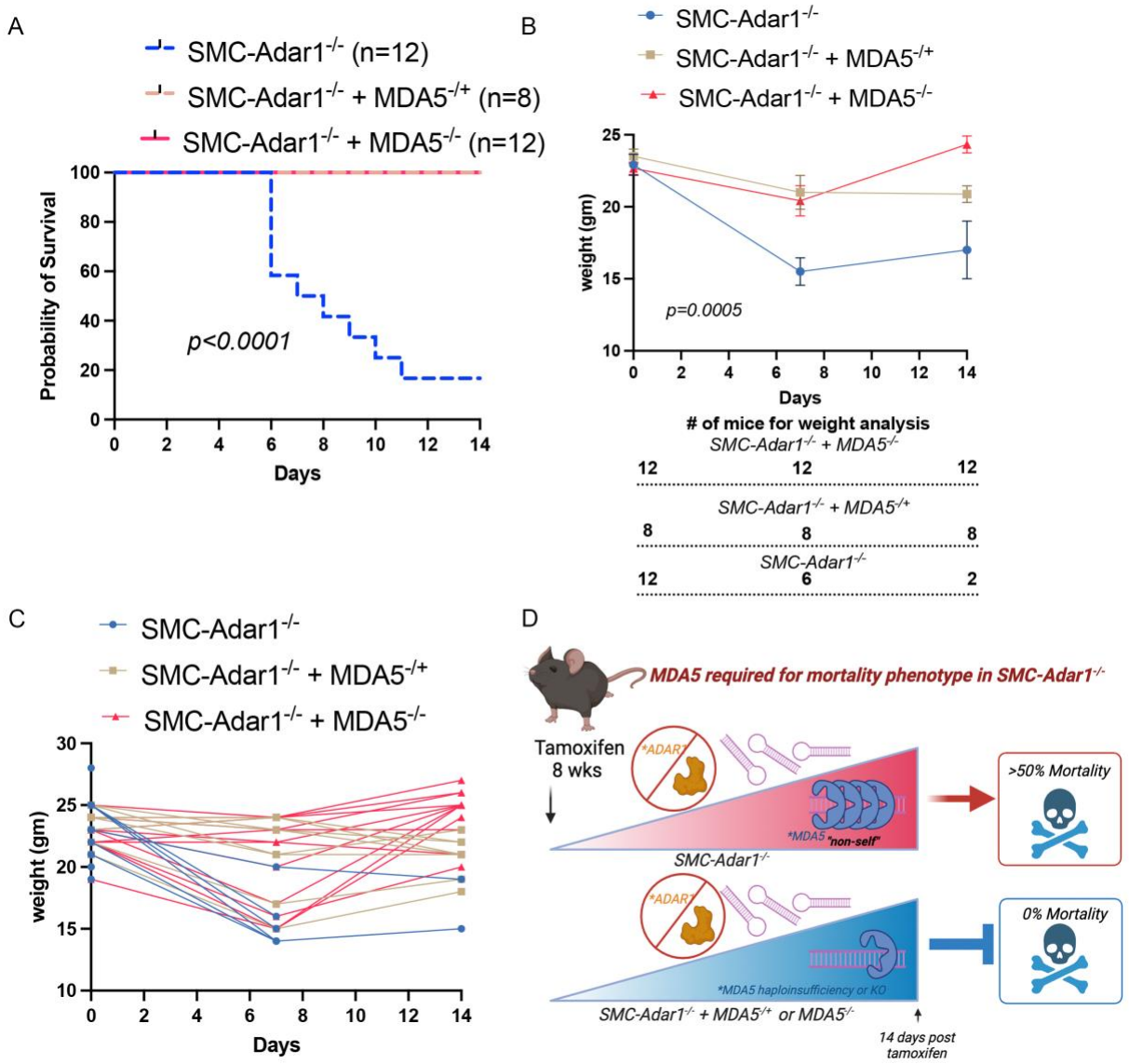

Figure 3. *Haploinsufficiency in MDA5 is adequate to prevent mortality in SMC-Adar1$^{-/-}$ mice.* (A) Survival curves for *SMC-Adar1$^{-/-}$* (*Adar1$^{fl/fl}$*, *Myh11^{CreERT2}*, *ROSAtdTomato*, *ApoE$^{-/-}$*), *SMC-Adar1$^{-/-}$*, *MDA5$^{-/+}$* (*Adar1$^{fl/fl}$*, *Ifih1$^{-/+}$*, *Myh11^{CreERT2}*, *ROSAtdTomato*, *ApoE$^{-/-}$*), and *SMC-Adar1$^{-/-}$*, *MDA5$^{-/-}$* (*Adar1$^{fl/fl}$*, *Ifih1$^{-/-}$*, *Myh11^{CreERT2}*, *ROSAtdTomato*, *ApoE$^{-/-}$*) genotypes following tamoxifen treatment at 8 weeks of age. (B) Weight curve at 0, 7, and 14 days following tamoxifen treatment between genotypes of surviving mice. (C) Individual weight measures at 0, 7, and 14 days following tamoxifen treatment between genotypes of surviving mice. (D) Schematic diagram of *SMC-Adar1$^{-/-}$* and MDA5 haploinsufficiency or global KO protecting against mortality. *P-*

1509 values represent comparison of survival curves Log-rank (Mantel-Cox) test (A-B). (B)

1510 Data point represents means (±SEM).

1511

1512

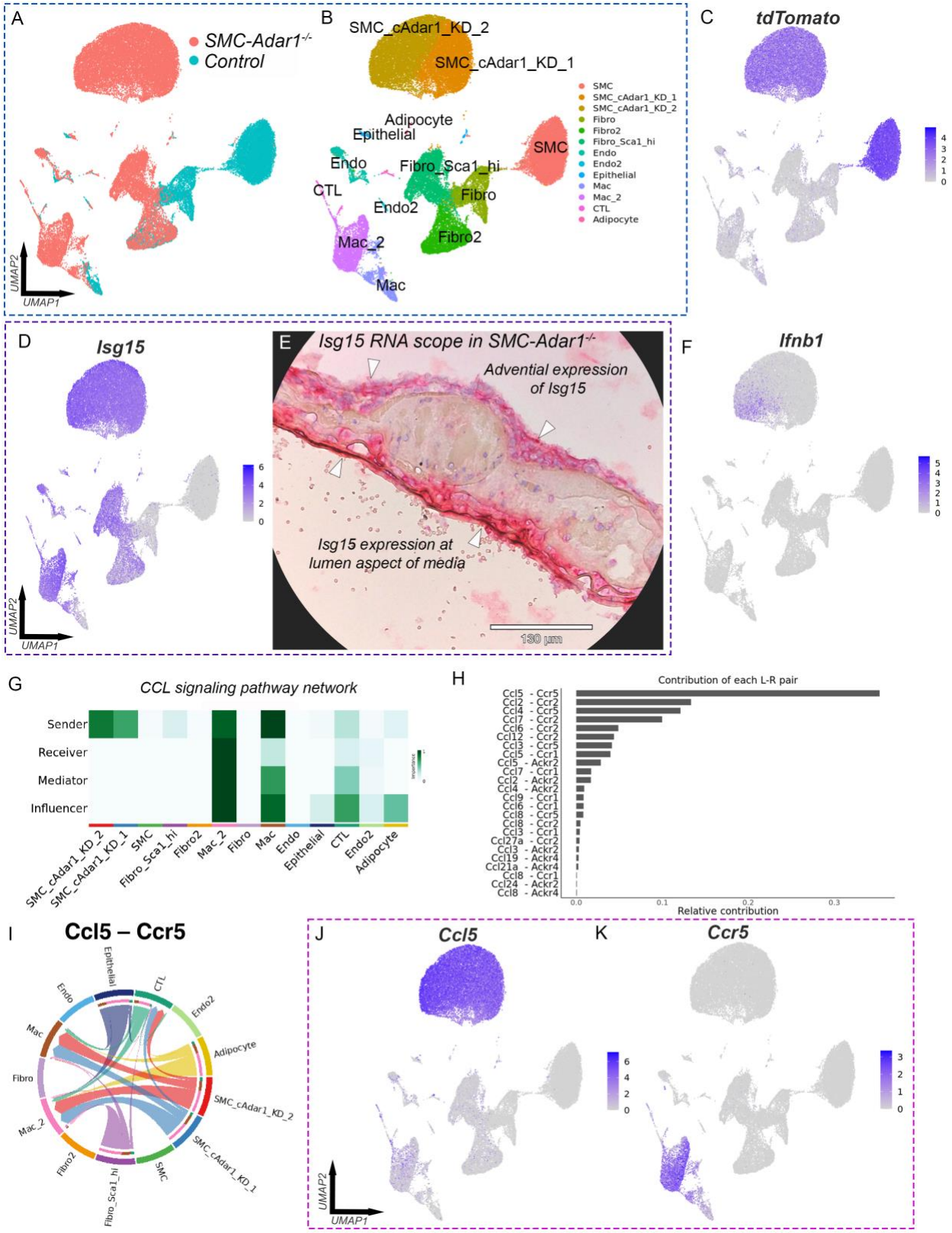

Figure 4. ***Single cell RNA sequencing reveals SMC Adar1 to control ISG activation, phenotypic response, and macrophage infiltration*****.** (A) scRNAseq

1516 UMAP from aortic root and ascending aorta grouped by genotype of *SMC-Adar1*$^{-/-}$
1517 (*Adar1*$^{fl/fl}$, *Myh11*^{CreERT2}, *ROSAtdTomato*, *ApoE*$^{-/-}$) and control (*Adar1*$^{WT/WT}$, *Myh11*^{CreERT2},
1518 *ROSAtdTomato*, *ApoE*$^{-/-}$) genotypes at 2 weeks following tamoxifen treatment. (B)
1519 UMAP with clustering and cell type identification of combined *SMC-Adar1*$^{-/-}$ and control
1520 genotype data. (C) Featureplot of tdTomato showing SMC lineage tracing. (D)
1521 Featureplot of *Isg15*. (E) RNAscope of *Isg15* in aortic tissue of *SMC-Adar1*$^{-/-}$ mice
1522 showing highest *Isg15* expression at the lumen aspect of media, with additional
1523 adventitial expression. (F) Featureplot of *Ifnb1*. (G) Heatmap of network centrality
1524 scores for CCL signaling network across cell clusters. (H) Contributions of each
1525 receptor-ligand pair for CCL signaling. (I) Chord diagram of receptor-ligand interaction
1526 between clusters for CCL5:CCR5. (J-K) Featureplot of (J) *Ccl5* and (K) *Ccr5*.
1527

1528

1529

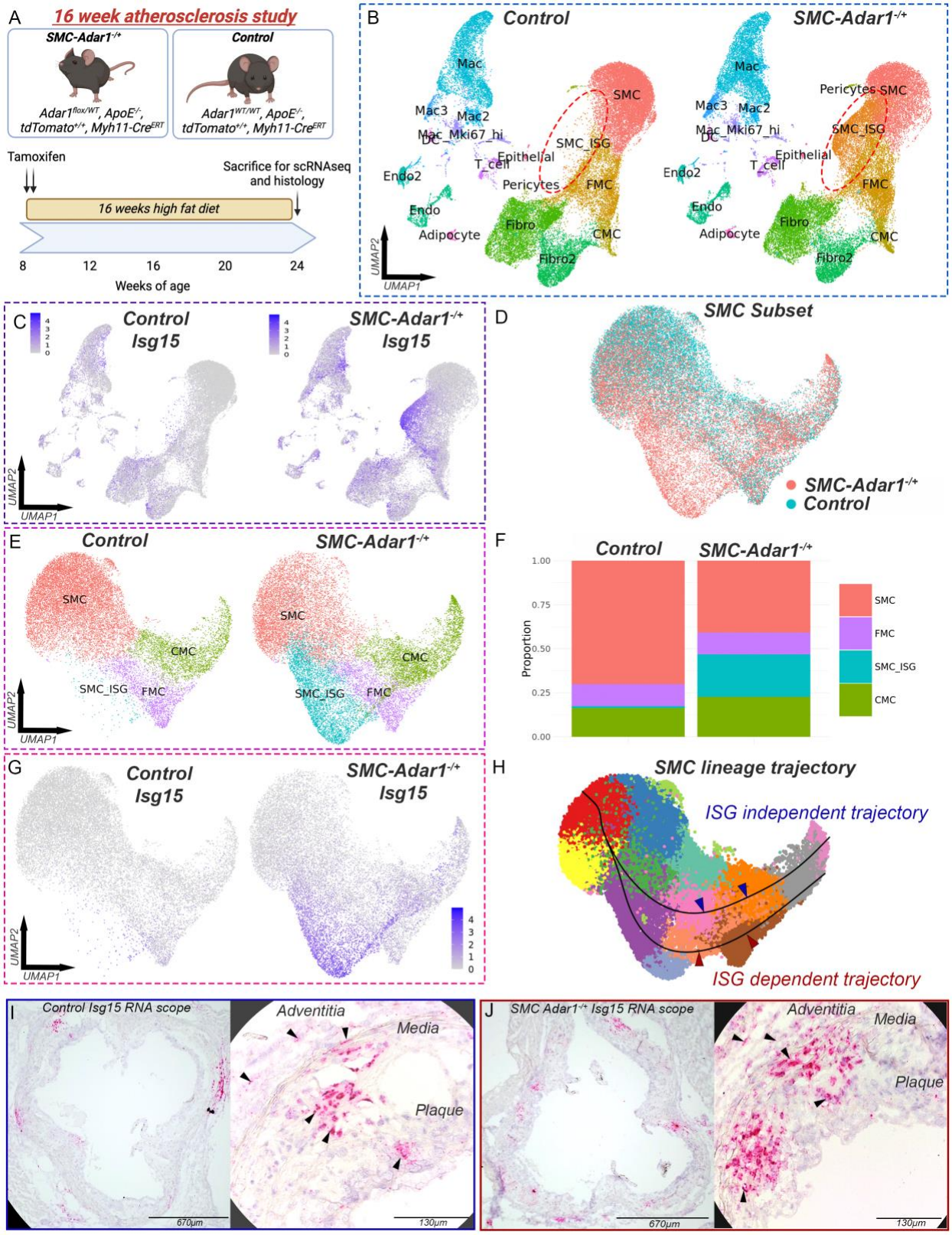

1530

1531 **Figure 5.** ***SMC specific haploinsufficiency of Adar1 activates the ISG response in***
1532 ***atherosclerosis increasing vascular chondromyoctye formation.*** (A) Schematic
1533 diagram of 16 week high fat diet (HFD) atherosclerosis study. (B) UMAP of scRNAseq
1534 data from atherosclerotic aortic root and ascending aorta at 16 weeks high fat diet split
1535 by control (*Adar1*$^{WT/WT}$, *Myh11*^{CreERT2}, *ROSAtdTomato*, *ApoE*$^{-/-}$) and *SMC-Adar1*$^{-/+}$
1536 (*Adar1*$^{fl/WT}$, *Myh11*^{CreERT2}, *ROSAtdTomato*, *ApoE*$^{-/-}$) genotypes. (C) Featureplot of *Isg15*
1537 split by genotype. (D) UMAP of SMC subset analysis grouped by genotype. (E) UMAP
1538 of SMC subset cluster analysis split by genotype showing SMC, SMC_ISG (interferon
1539 stimulated gene), fibromyocyte (FMC), and chondromyocyte (CMC) cell clusters. (F)
1540 Stacked bar chart showing cell populations of SMC subset for SMC, SMC_ISG, FMC,
1541 and CMC clusters. (G) Featureplot of *Isg15* in SMC subset split by genotype. (H)
1542 Lineage trajectory analysis using slingshot within SMC subset showing two distinct
1543 lineages (SMC_ISG dependent and independent) from SMC to CMC. (I&J) RNA scope
1544 for *Isg15* in aortic root sections in control (I) and *SMC-Adar1*$^{-/+}$ (J) mice.
1545

1546

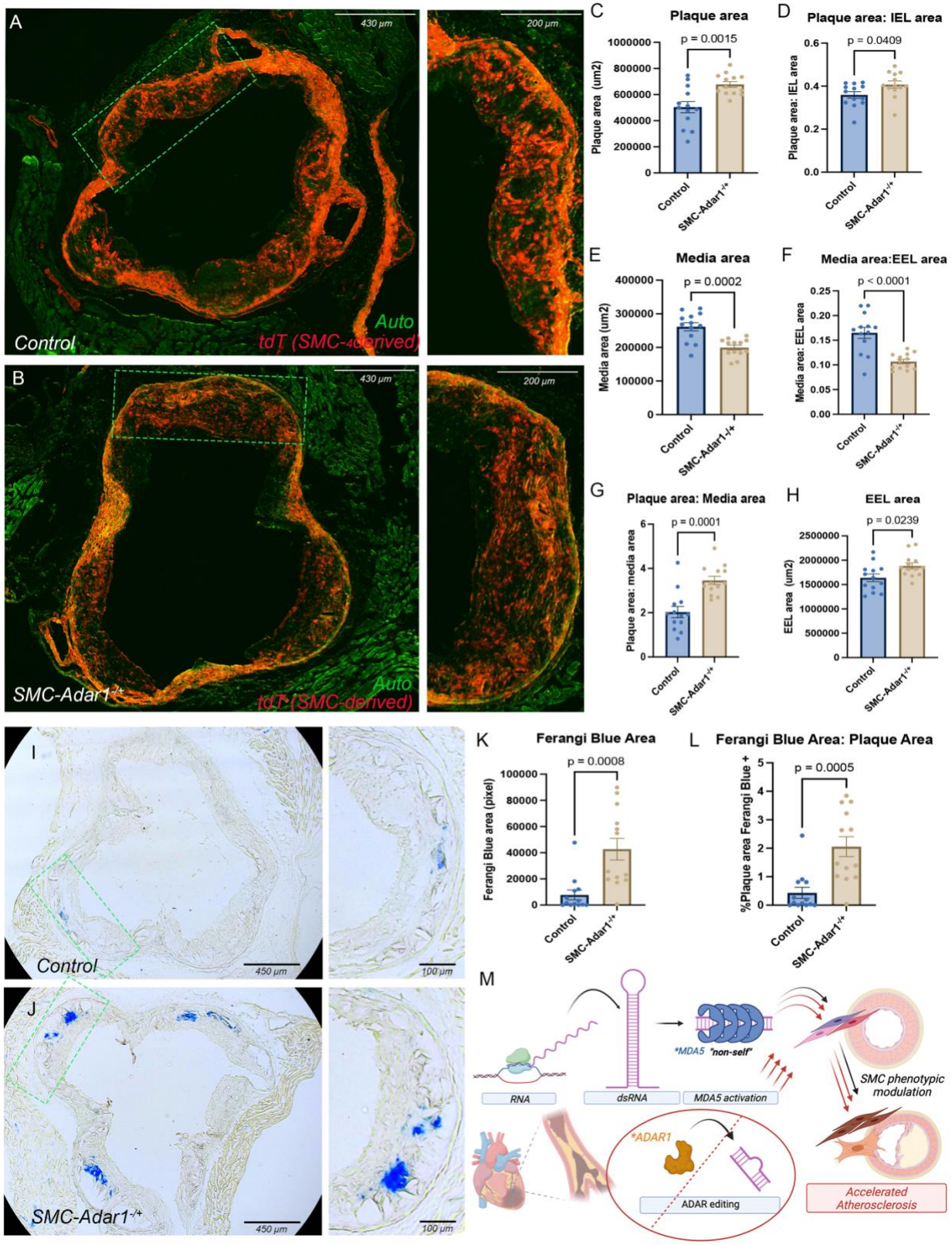
A
430 µm
200 µm
Control
Auto
tdT (SMC-derived)
B
SMC-Adar1-/+
C
Plaque area
p = 0.0015
Plaque area (um2)
D
Plaque area: IEL area
p = 0.0409
Plaque area: IEL area
E
Media area
p = 0.0002
Media area (um2)
F
Media area:EEL area
p < 0.0001
Media area: EEL area
G
Plaque area: Media area
p = 0.0001
Plaque area: media area
H
EEL area
p = 0.0239
EEL area (um2)
Control
SMC-Adar1-/+
I
450 µm
100 µm
J
K
Ferangi Blue Area
p = 0.0008
Ferangi Blue area (pixel)
L
Ferangi Blue Area: Plaque Area
p = 0.0005
%Plaque area Ferangi Blue +
M
RNA
dsRNA
MDA5 activation
*MDA5
"non-self"
SMC phenotypic modulation
*ADAR1
ADAR editing
Accelerated Atherosclerosis

1547

1548 **Figure 6.** ***SMC specific haploinsufficiency in Adar1 increases plaque size and***
1549 ***calcification in atherosclerosis.*** Representative fluorescent images of aortic root
1550 plaque histology in *SMC-Adar1*$^{-/+}$ and control genotypes (A&B) with quantification of
1551 plaque area (C), plaque area normalized to internal elastic lamina area (IEL) (D), media
1552 area (E), media area normalized to external elastic lamina area (EEL) (F), plaque area
1553 normalized to media area (G), and EEL area (H). Representative images of Ferangi
1554 Blue calcification staining in *SMC-Adar1*$^{-/+}$ and control genotypes (I&J), quantification of
1555 Ferangi Blue area (K), and Ferangi Blue area normalized to plaque area (L). (M)
1556 Schematic diagram showing mechanism of dsRNA formation, MDA5 activation, and
1557 impaired RNA editing by ADAR1 to accelerate SMC phenotypic modulation,
1558 calcification, and atherosclerosis. Data represent mean +/- SEM, N = 13 per group. *P*-
1559 values represent unpaired two-tailed T-test.
1560
1561
1562

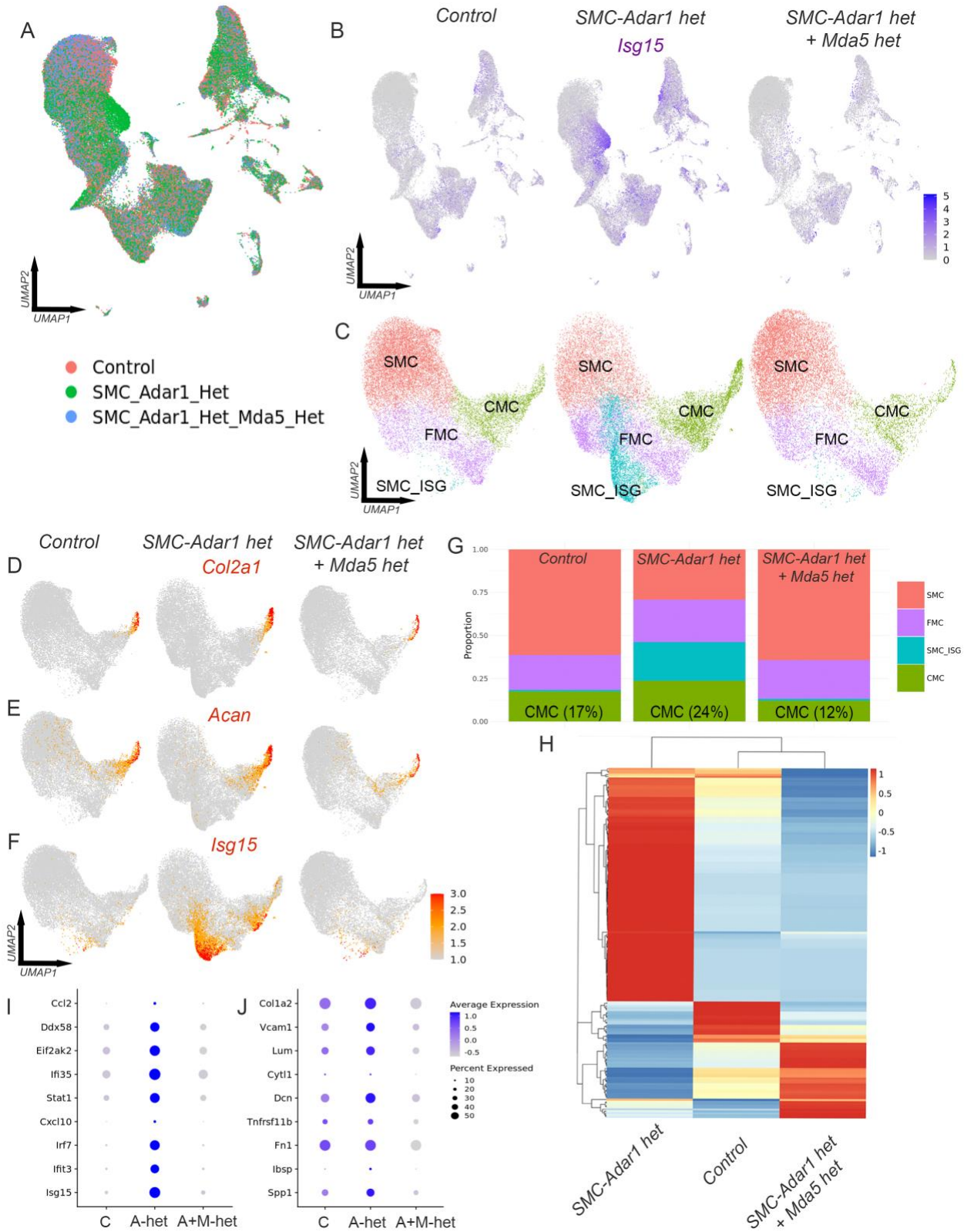

Figure 7. ***Haploinsufficiency of Mda5 prevents ISG activation and chondromyocyte formation in atherosclerosis with SMC-Adar1$^{-/+}$.*** (A) UMAP of

integrated scRNAseq data set between control (*Adar1*$^{WT/WT}$, *Myh11*^{CreERT2}, *ROSAtdTomato, ApoE*$^{-/-}$), *SMC-Adar1 het* (*Adar1*^{flWTl}, *Myh11*^{CreERT2}, *ROSAtdTomato, ApoE*$^{-/-}$), and *SMC-Adar1 het + Mda5 het* (*Adar1*^{flWTl}, *Ifih1*$^{-/+}$, *Myh11*^{CreERT2}, *ROSAtdTomato, ApoE*$^{-/-}$) genotypes following 16 weeks high fat diet. (B) Featureplot of *Isg15* split by genotype. (C) UMAP tdTomato+ subset analysis with SMC, SMC_ISG, FMC, and CMC clusters split by genotype. Featureplots split by genotype for (D) *Col2a1*, (E) *Acan*, and (F) *Isg15*. (G) Stacked bar charts showing proportion of cells within 'SMC', 'SMC_ISG', 'FMC', and 'CMC' clusters split by genotype. (H) Heatmap visualization for normalized expression of marker genes for control, *SMC-Adar1 het*, and *SMC-Adar1 het + Mda5 het* genotypes in tdTomato+ subset analysis. Dotplot gene expression splity by genotype in SMC subset for (I) ISG genes and (J) FMC/CMC marker genes.

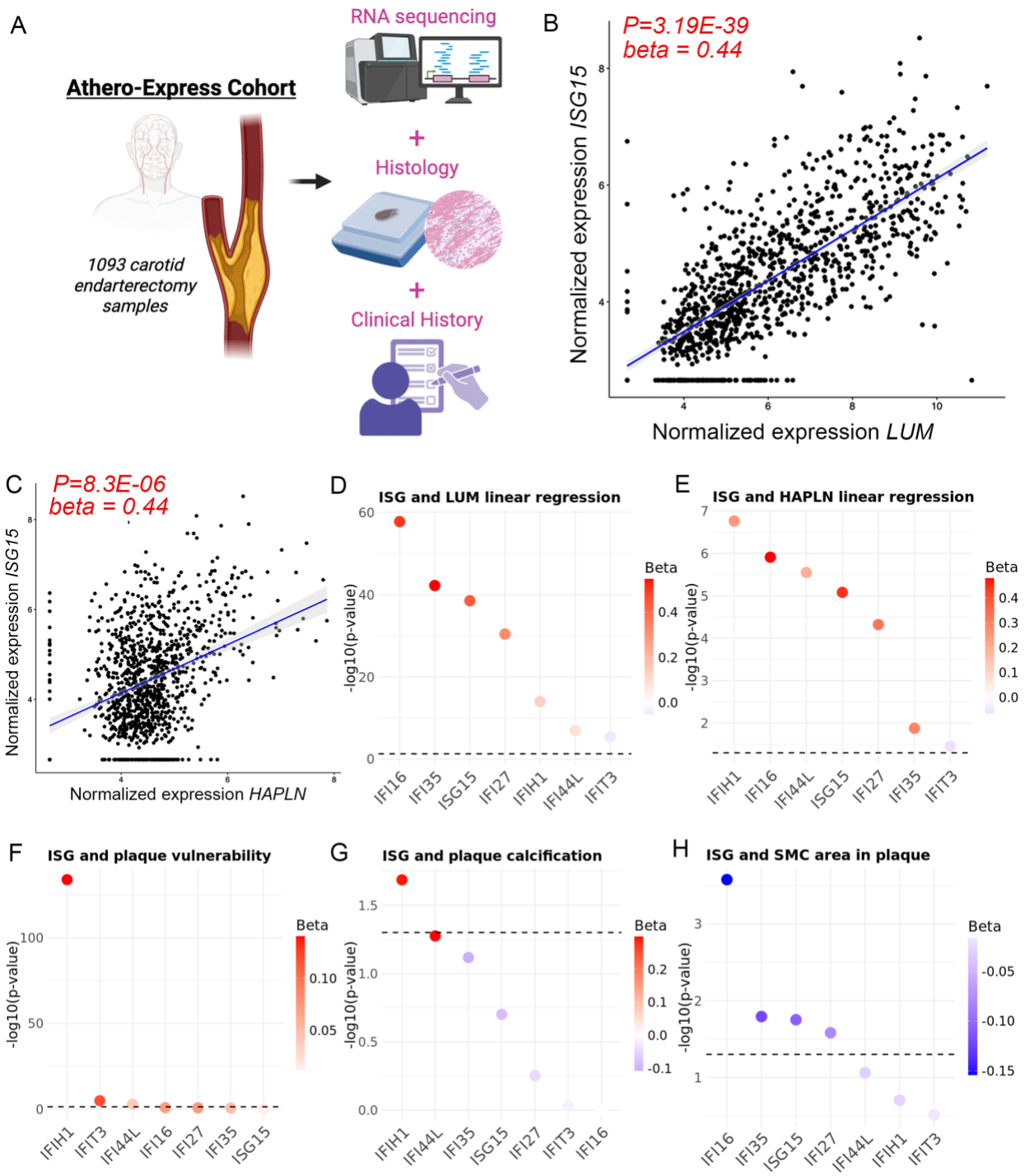

Figure 8. ***ISG expression in human atherosclerotic plaque dataset (Athero-Express) correlates to markers of SMC modulation, plaque vulnerability, plaque calcification, and decreasing SMC investment into plaque.*** (A) Schematic diagram of Athero-Express cohort and data evaluation. Linear relationship analysis between chondromyocyte markers *LUM* (B) and *HAPLN* (C) to *ISG15*. Dot plots displaying linear

1587 regression analysis between ISGs and *LUM* (D) and *HAPLN* (E) showing -log10(p
1588 value) on Y axis and gene on X axis with beta coefficient scaled by color. Dot plots
1589 displaying linear regression analysis between ISGs and plaque phenotype corrected for
1590 co-variates for (F) plaque vulnerability, (G) calcification, and (H) SMC area within
1591 plaque.